Chapter 4

Electron transfer dynamics

Within this chapter time-resolved measurements of the electron injection as well as the recombination are described. The influence of the chemical nature of the bridge-anchor unit, properties of the semiconductor, effects of the preparation procedure, and finally effects of a solvent environment compared to UHV conditions are discussed.

4.1 Strong coupling case: DTB-Pe-COOH on TiO_2

First, the case of perylene directly linked to the surface via a carboxylic group is discussed. This dye will be treated as a reference system for the perylene derivatives with different bridge-anchor units. Fig. 4.1 shows the transient absorption at 565 nm with a spectral resolution of 2 nm after excitation with a pump pulse centered at 435 nm. The transient absorption reflects the rise of the molecular product of the heterogeneous ET. The striking conclusion from Fig. 4.1 is that the ET occurs with a rate above $5{\times}10^{13}$/s. Data fitting with a rate equation model reveals a time constant of 13 fs.
In terms of molecular vibrations an oscillation period of 13 fs corresponds to a mode with $\hbar\omega_{vib} \approx 2550$ cm^{-1}. The highest vibrational modes of the perylene backbone are around 1600 cm^{-1} (see section 3.3). Thus the electron injection from DTB-Pe-COOH is definitely faster than the highest vibrational modes of the chromophore.
Before the ET mechanism will be considered in section 4.1.2 some general aspects of the pump-probe signals and features displayed by the transient of DTB-Pe-COOH are discussed, as they are exemplary also for the other perylene chromophores.

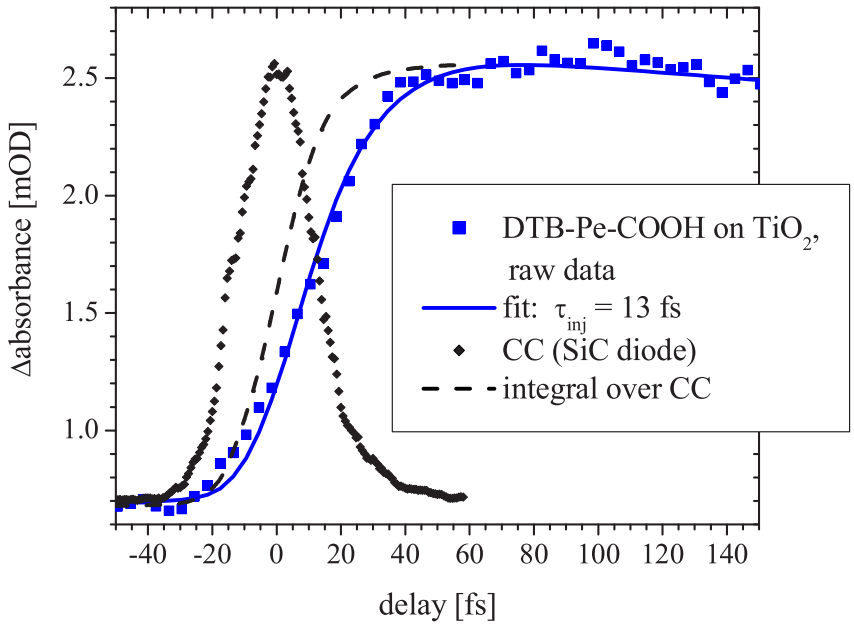

Figure 4.1: ET transfer kinetics of DTB-Pe-COOH: raw transient absorption data (squares) of the molecular product state of the electron transfer (perylene cation) taken at 565 nm after excitation with a sub-20 fs pump pulse centered at 435 nm. The measurement was performed in UHV. The fit of the data according to Eq. 4.8 is given as a solid line and reveals a time constant τ_{inj} of 13 fs. The cross-correlation (CC) and its integral are given as diamonds and dashed line, respectively.

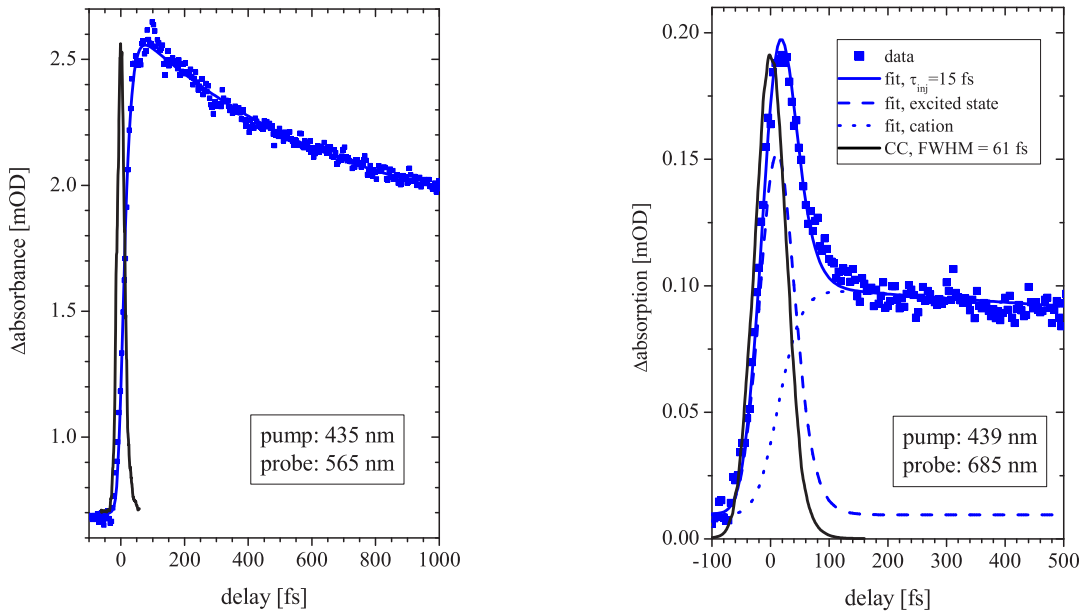

Figure 4.2: Left panel: Same data as shown above for a different time range. Right panel: Transient absorption at 685 nm which is a superposition of excited state absorption and cation absorption.

4.1.1 General aspects of the transient absorption measurements

4.1.1.1 Assignment of the 570 nm signal

The benefits of the absorption spectra of perylene have been discussed in section 3.1 (see Fig. 3.1). The transient absorption signal around 570 nm can be purely ascribed to the perylene cation absorption and thus directly reflects the course of the ET. This assignment has been examined before for DTB-Pe-CH_2-P(O)$(OH)_2$: the electron injection from this dye into a nano-structured TiO_2 anatase film was time-resolved by measuring different transient absorption signals, firstly the decay of the excited singlet state at 715 nm [19, 118], secondly the rise in the population of the ionized state by probing the perylene cation $D_0 \rightarrow D_5$ transition [131, 122] around 570 nm [19, 118], and thirdly the rise in the population of the injected electrons measured as intra-band transitions at 1325 nm [118]. The three different signals gave the same mono-exponential charge transfer rate.

To test the validity of these results also for the stronger coupled DTB-Pe-COOH transient absorption at 685 nm has been measured. At that spectral position the excited state absorption and the cation absorption superimpose. As displayed in the right panel of Fig. 4.2 the time trace shows some instantaneous signal rising with the system function and a subsequent fast decay to a certain level. The transient absorption can be fitted with a simple rate equation model (see the following section) that describes both excited state and cation signal, resulting in a time constant of 15 fs.

These results ensure sufficient confidence for identifying the rise in the population of the ionized state of the perylene chromophore with the time dependence of the electron injection process.

4.1.1.2 Data fitting - rate equation model

The simplest approach to describe photoexcitation and population transfer between states is following Einsteins rate equation description of the atom field interaction [183]. The rate equation model describing an electron transfer system investigated with pump-probe spectroscopy is illustrated in Fig. 4.3. The photoexcited state decays exponentially into the cationic state due to electron injection with a rate $\gamma_{inj} = \tau_{inj}^{-1}$. The cationic state decays exponentially with the time constant τ_{rec} due to recombination. The time dependence of the excited state population $N_{exc}(t)$

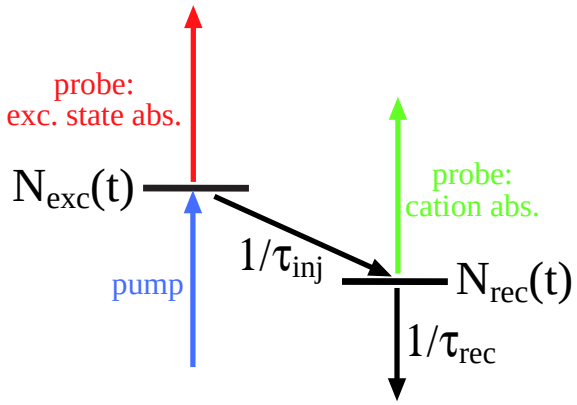

Figure 4.3: Schematic illustration of the rate equation model.

and the perylene cation population $N_{cat}(t)$ is given by the differential equations

$$\dot{N}_{exc}(t) = I_0 I_{pump}(t) - N_{exc}(t)/\tau_{inj} \ , \tag{4.1}$$

$$\dot{N}_{rec}(t) = N_{exc}(t)/\tau_{inj} - N_{cat}(t)/\tau_{rec} \ , \tag{4.2}$$

where $I_{pump}(t)$ denotes the instantaneous intensity of the pump pulse and I_0 a constant prefactor. $I_{pump}(t)$, the source term, is proportional to the square of the envelope of the pump field, the rapid oscillations of the field are neglected. In the rate equation description the pump-probe signal $I_{pp}(t_d)$ is described by the integral of the product of the probe instantaneous intensity $I_{probe}(t - t_d)$ and the population of the state of interest, i.e. for the cation absorption

$$I_{pp}^{cat}(t_d) = \int_{-\infty}^{\infty} I_{probe}(t - t_d) N_{cat}(t) dt. \tag{4.3}$$

t_d denominates the time delay between the pump and the probe pulse. As $I_{pump}(t)$ is usually assumed to be Gaussian or $sech^2$ shaped there is no analytical solution for Eq. 4.1 and 4.2, if the error function is not assumed as analytical. But as there is only one source term the populations $N_{exc}(t)$ and $N_{cat}(t)$ can be obtained by the convolution of $I_{pump}(t)$ with the analytical solutions $\tilde{N}_{exc}(t)$ and $\tilde{N}_{cat}(t)$ of Eq. 4.1 and 4.2 without the source term. The latter reads

$$\tilde{N}_{exc}(t) = N_0 \, e^{\frac{t}{\tau_{inj}}} \ , \tag{4.4}$$

$$\tilde{N}_{cat}(t) = N_0 \frac{\tau_{rec}}{\tau_{rec} - \tau_{inj}} (e^{-\frac{t}{\tau_{rec}}} - e^{-\frac{t}{\tau_{inj}}}) \ , \tag{4.5}$$

for the initial conditions $N_{exc}(0) = N_0$ and $N_{cat}(0) = 0$. The populations are thus

$$N_{exc}(t) = \int_{-\infty}^{\infty} I_{pump}(t - t') \tilde{N}_{exc}(t') \, dt', \tag{4.6}$$

$$N_{cat}(t) = \int_{-\infty}^{\infty} I_{pump}(t - t') \tilde{N}_{cat}(t') \, dt'. \tag{4.7}$$

Inserting Eq. 4.6 and 4.7 in Eq. 4.3 yields

$$\begin{aligned} I_{pp}^{cat}(t_d) &= \int_{-\infty}^{\infty} I_{probe}(t-t_d) \int_{-\infty}^{\infty} I_{pump}(t-t')\tilde{N}_{cat}(t')dt'dt \\ &= \int_{-\infty}^{\infty} \tilde{N}_{cat}(t') \int_{-\infty}^{\infty} I_{probe}(t-t_d) I_{pump}(t-t')dtdt' \ . \end{aligned} \tag{4.8}$$

The commutation of the integrations in Eq. 4.8 inverses the sequence of convolutions, i.e. firstly the pump and the probe pulses are convoluted. Experimentally this corresponds to a second-order cross-correlation measurement. According to Eq. 4.8 the transient absorption signal can be fitted by convoluting the experimental CC with the solution of the appropriate rate equation model without the source term (Eq. 4.4 and 4.5). This is the simplest data fitting method for pump-probe signals and works generally well for kinetics slower than the system function of the experiment. However, electron injection can occur on the sub-20 fs timescale, as shown in Fig. 4.1, i.e. the main kinetics occur while pump and probe pulses overlap in time. In this situation the coherent nature of the photoexcitation, which is neglected in the rate equation model, and coherent contributions to the transient absorption signal have to be considered. This will be discussed in the following two paragraphs.

4.1.1.3 Data fitting - optical Bloch equations

The quantum mechanical description of field-matter interaction is usually formulated in terms of the density matrix $\boldsymbol{\rho}$ [183, 184]. This allows the incorporation of dephasing effects. The temporal evolution of the density matrix is given by the Liouville equation [185]

$$\dot{\boldsymbol{\rho}} = -\frac{i}{\hbar}[H_0 + V(t), \boldsymbol{\rho}] - \Gamma\boldsymbol{\rho}, \tag{4.9}$$

where H_0 denotes the Hamiltonian of the undisturbed system, $V(t)$ the interaction with the electric field, and $\Gamma\boldsymbol{\rho}$ a phenomenological relaxation matrix. Eq. 4.9 is conveniently solved within the rotating frame approximation, resulting in the optical Bloch equations (OBE) [183, 186]. The OBE describe the temporal evolution of the populations and polarizations induced by the electric field. For example, the OBE allow the simulation of quantum beats at metal surfaces observed by time-resolved photoelectron spectroscopy [187, 188]. For the same system Hertel and co-workers discussed the difference between a rate equation description and the OBE for the time-dependent population of an excited state in a 2-level system [189].

For a pump-probe experiment on heterogeneous ET with the cation absorption as the probe transition, four levels have to be considered. This is illustrated in Fig. 4.4: The levels $|1>$ and $|2>$, ground and excited state of the neutral molecule, are coupled

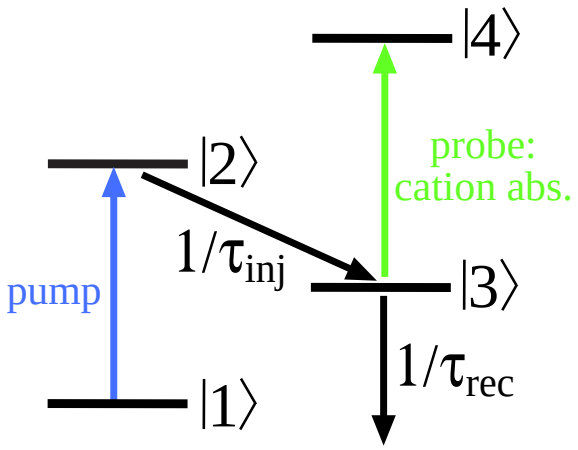

Figure 4.4: Schematic illustration of the 4-level system modeled with the optical Bloch equations (OBE).

by the pump field. The electron injection is considered as an *incoherent* coupling of the excited state to the cation ground state $|3>$ (the population relaxation time T_1 of the excited state is thus τ_{inj}). The probe field couples $|3>$ and the cationic excited state $|4>$. The model is not a true 4-level system as no coherence between the neutral and cationic moieties are allowed. It should be seen as two incoherently coupled 2-level systems. An example of multilevel OBE (with 20 states of sodium) is given by Ref. [190]. Setting up the OBE for our system within the rotating wave and dipole approximations and with the restriction to purely resonant transitions reveals:

$$\dot{\rho_{22}} = \frac{\mu_{12}E_{pump}(t)}{2i\hbar}(\rho_{12} - \rho_{21}) - \frac{\rho_{22}}{\tau_{inj}} \tag{4.10}$$

$$\dot{\rho_{12}} = \frac{\mu_{12}E_{pump}(t)}{2i\hbar}(\rho_{22} - 1) - \frac{\rho_{12}}{T_2^{(1)}} \tag{4.11}$$

$$\dot{\rho_{33}} = -\frac{\mu_{34}E_{probe}(t-t_d)}{2i\hbar}(\rho_{34} - \rho_{43}) + \frac{\rho_{22}}{\tau_{inj}} - \frac{\rho_{33}}{\tau_{rec}} \tag{4.12}$$

$$\dot{\rho_{34}} = \frac{\mu_{34}E_{probe}(t-t_d)}{2i\hbar}(\rho_{44} - \rho_{33}) + \frac{\rho_{34}}{T_2^{(2)}} \tag{4.13}$$

$$\dot{\rho_{44}} = \frac{\mu_{34}E_{probe}(t-t_d)}{2i\hbar}(\rho_{34} - \rho_{43}). \tag{4.14}$$

The diagonal terms of $\boldsymbol{\rho}$ are real numbers and give the time-dependent populations of the states, whereas the imaginary off-diagonal terms give the particular coherences. $E_{pump}(t)$ and $E_{probe}(t-t_d)$ denote the envelopes of the electric fields, which should not be confused with the instantaneous intensity $\propto E^2$ used in the rate equation model. Although the frequencies of the fields are not specified it is assumed that both fields are spectrally separated. An additional assumption is that the pump field is weak and the ρ_{44} population relaxation time is long compared to the width

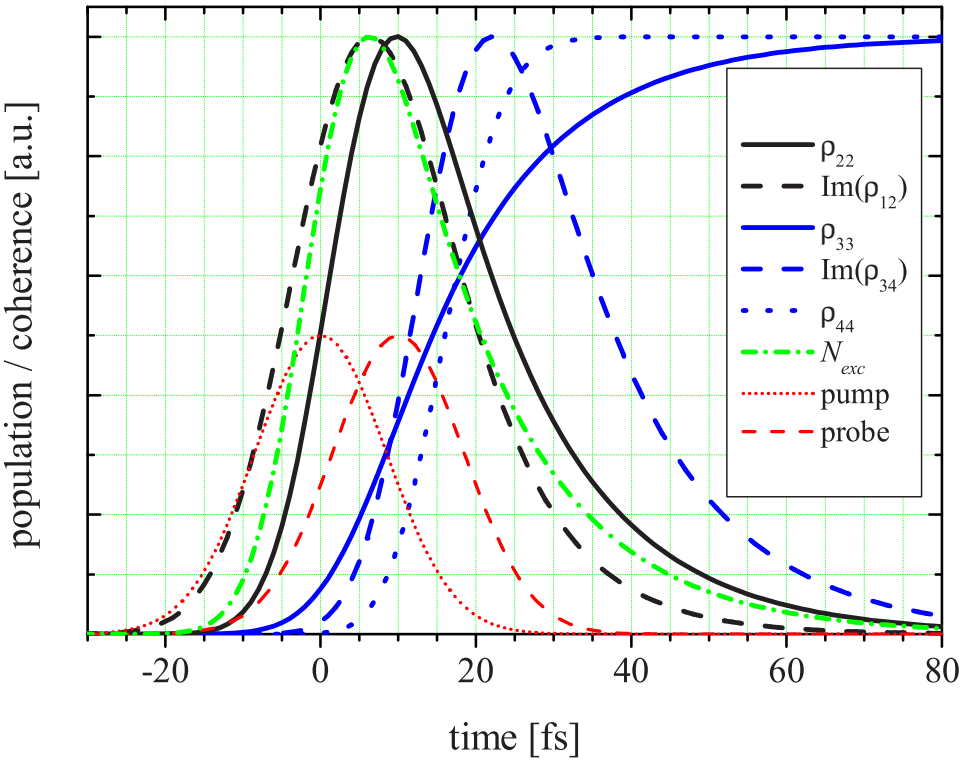

Figure 4.5: Solutions of the optical Bloch equations defined in Eq. 4.10 - 4.14 for $\tau_{inj} = T_2^{(1)*} = T_2^{(2)*} = 15$ fs, $\tau_{rec} = \infty$. As an example the delay has been chosen as $t_d = 10$ fs. Pump and probe fields (red lines) are Gaussians of 20 fs FWHM (i.e. the FWHM of the instantaneous intensity is 14.1 fs). The black lines give the population of the photoexcited state (solid line) and the coherence induced by the pump field (dashed line). The 15 fs-ET process populates the cation ground state ρ_{33} (blue solid line). The probe field generates the coherence ρ_{34} (blue dashed line) and transfers population into the cationic excited state ρ_{44} (blue dotted line). All curves are normalized. The green dash-dotted line gives $N_{exc}(t)$ according to the rate equation model for comparison with ρ_{22}.

of the probe pulse. Both assumptions are fulfilled in the experiment[1]. $T_2^{(1)} = (1/2\tau_{inj} + 1/T_2^{(1)*})^{-1}$ is the dephasing in the neutral molecule, where $T_2^{(1)*}$ represents the "pure" dephasing. For the cationic states the dephasing is determined by the pure dephasing ($T_2^{(2)} \approx T_2^{(2)*}$), as the population relaxation of both states can be assumed to be slow compared to the dephasing.

The pure dephasing times $T_2^{(1)*}$ and $T_2^{(2)*}$ are unknown. The time scale of electronic dephasing is strongly system dependent and ranges from tens of femtoseconds for large molecules in solution (see for example Refs. [192, 193]) to hundreds of picosec-

[1] 1. The center frequencies of the pump and the probe pulses are separated by about 5500 cm^{-1}. 2. The energetic position of the cationic excited state can be estimated to be in the band gap of the semiconductor or below. Therefore ET from that state to the surface can be excluded. The lifetime of the cation excited state is in the tens of picoseconds range [191].

onds for small molecules in the gas phase [194]. For the case of a large adsorbate protruding into vacuum, but bound to a surface, electronic dephasing has not been investigated so far[2]. In this situation the high electronic density of the solid around the molecular excited state will affect the dephasing time, rather than the absence of a proximate environment. Thus it is likely that dephasing occurs on the ultrafast time scale, eventually even faster than dephasing induced by high frequency fluctuations of a surrounding bath.

To gather insight into the temporal evolution of the density matrix its elements are plotted in Fig. 4.5 for Gaussian pump and probe fields of 20 fs FWHM with t_d=10 fs, indicated as red lines. The population relaxation time (i.e. electron injection) and the pure dephasing time T_2^* for the total system are assumed as 15 fs. Recombination and injection from the excited cationic state are neglected. For the neutral and the oxidized molecule T_2 is thus 10 and 15 fs, respectively. The products $\mu_{12}E_{pump}(t=0)$ and $\mu_{34}E_{probe}(t=t_d)$ are treated as constants. The values are chosen such that no saturation or depopulation effects occur, which reflects the experimental situation. Quantitatively this means that the populations transfered by the fields are less than 1% of the ground state populations in both cases.

The black curves show the evolution of the polarization $\mathrm{Im}(\rho_{12})$ (dashed line) induced by the pump field and the population ρ_{22} of the excited state. Due to the fast population decay caused by electron injection both time traces have similar shapes, but the population follows the coherence with a delay of 4-5 fs. The excited state decay is mirrored by the build-up of the cation ground state population ρ_{33} (blue solid line). So far the density matrix is independent of the probe field. It is interesting to note, that the excited state population $N_{exc}(t)$ according to the rate equation model (Eq. 4.6), indicated as green dash-dotted line (FWHM of $I_{pump}(t)$: 14.14 fs), lies in-between the coherence and the population.

In the cation moiety the presence of a probe pulse creates the coherence $\mathrm{Im}(\rho_{34})$ (blue dashed line) and transfers some population ρ_{44} (blue dotted line) into the cation excited state. Because of the longer dephasing time (no population relaxation of the excited state) the coherence $\mathrm{Im}(\rho_{34})$ decays slightly slower compared to $\mathrm{Im}(\rho_{12})$. With respect to pump-probe spectroscopy the crucial property now is $\mathrm{Im}(\rho_{34})$, as it reflects the sequential part (with field order pump-pump-probe) of the 3rd-order polarization. The pump-probe signal $I_{pp}(t_d)$ is the polarization $P^{(3)}(t,t_d)$ induced

[2]Petek and co-workers reported an electronic dephasing time of 15 fs for an atomic adsorbate (CS) on a metal surfaces (Cu (111)) at low temperatures [195].

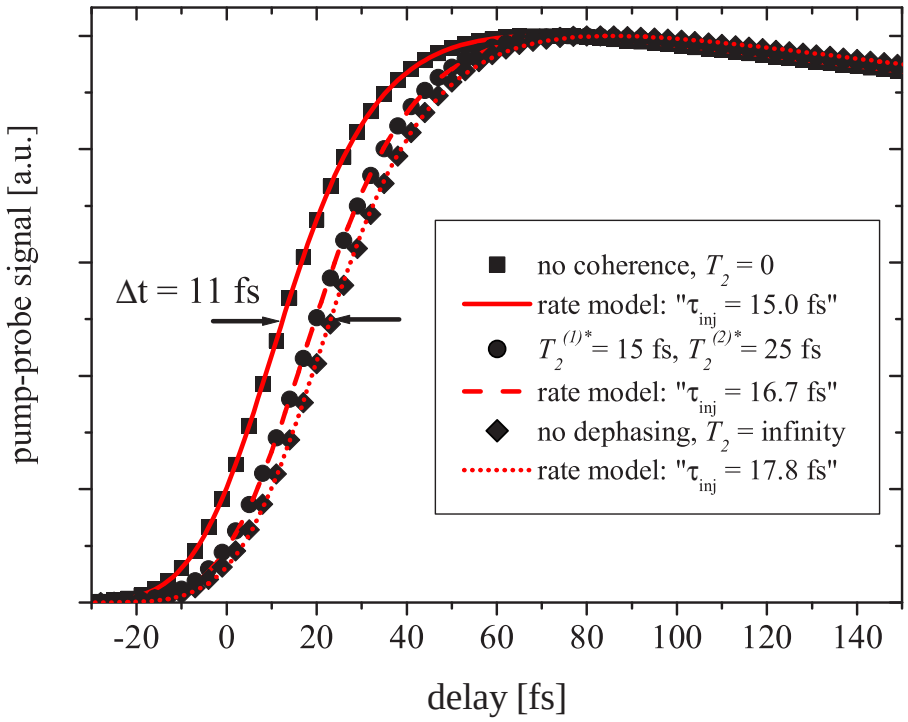

Figure 4.6: Comparison of the rate equation model with optical Bloch equations: Normalized pump-probe signals $I^{cat}_{pp,seq}(t_d)$ for different situations: no coherence ($T_2 \to 0$, squares), no dephasing ($T_2 \to \infty$, diamonds), and an intermediate situation (circles, see legend and text). The red lines indicate least-square fits of the signal within the rate equation model.

in the probe transition heterodyned with the probe pulse [196]:

$$\begin{aligned} I^{cat}_{pp}(t_d) &= \int_{-\infty}^{\infty} \left[\left| E_{probe}(t,t_d) + iP^{(3)}(t,t_d) \right|^2 - \left| E_{probe}(t,t_d) \right|^2 \right] dt \\ &= 2\ \mathrm{Im} \int_{-\infty}^{\infty} \left(\mathrm{E_{probe}(t,t_d) P^{(3)}(t,t_d)} \right) . \end{aligned} \tag{4.15}$$

The sequential part of the signal $I^{cat}_{pp,seq}(t_d)$ can now be correlated with the coherence ρ_{34} obtained from the OBE:

$$I^{cat}_{pp,seq}(t_d) \propto \mathrm{Im} \left(\int_{-\infty}^{\infty} \mathrm{E_{probe}(t,t_d)} \rho_{34}(\mathrm{t}) \mathrm{dt} \right) . \tag{4.16}$$

Now we are set to take a look at the effect of the coherences on the pump-probe signals. Fig. 4.6 shows results of the OBE signal according to Eq.4.16 (scattered symbols) for the cases of no coherence ($T_2 \to 0$) (squares), no dephasing ($T_2 \to \infty$) (diamonds), and an intermediate situation with $T_2^{(1)*}$= 15 fs and $T_2^{(2)} = T_2^{(2)*}$= 25 fs (circles). The latter parameter choice might be the most realistic for the experimental situation. The time constants for electron injection τ_{inj} and recombination τ_{rec} have been chosen to be 15 fs and 1 ps, respectively. Pump and probe fields

are considered as Gaussians of 28.28 fs FWHM, adequate to a pulse duration of 20 fs. The time-dependent signals obtained in this way have been fitted with the rate equation model according to Eq. 4.8. The best fits are given as red lines. As expected, the OBE are exactely equivalent to the rate equation model for the situation of no coherence. In the case of coherence, the time traces look rather similar apart from a temporal shift, which can be as much as 11 fs (compared to $T_2 = 0$) for the chosen parameters. If the time-zero, i.e. the temporal position of the maximum of the system function, is allowed as free fit parameter, the rate equation model reproduces the OBE signal quite reasonable. The injection times obtained from the fit are 17.8 fs for the limit $T_2 \rightarrow \infty$ and 16.6 fs for the intermediate situation. For the latter case the rate equation model thus overestimates the injection time by about 10%.

However, if time-zero is kept fixed at the position determined by the cross-correlation measurement the rate equation model may overestimate the injection time by up to 60%. Within this fitting mode the failure of the rate equation model will depend on the method used for the determination of the CC. If the nonlinear signal is based on *nonresonant* transitions, which is usually the case, the measured CC maps the true time-zero of pump and probe pulses [189], and the error of the fit is maximumal. If *resonant* transitions are utilized, for instance the "instantaneous" rise of excited state absorption in a suitable dye, the time shift between the OBE and the rate equation model is at least partially incorporated in the determined time-zero. The error introduced by using the rate equation model for data fitting will be minor in this situation.

From this comparison the conclusion is drawn that the rate equation model describes the cation absorption sufficiently well, if *time-zero is allowed to be a free fit parameter*. As the rate equation model is much more convenient with respect to the computational time, it is used for data fitting in this work. In principle, the temporal shift of the signal with respect to the true time-zero could be utilized to gather information on the dephasing time. This has been pointed out recently within more advanced theoretical descriptions of pump-probe signals [197, 102]. But this requires a very reliable determination of time-zero measured at the sample position, i.e. in the UHV chamber. CC measurements outside the chamber might not be accurate enough. For instance the difference due to the dispersion in air outside the chamber compared to the dispersion-free path from the UHV window to the sample shifts time-zero by about 5 fs.

Nonresonant transitions have been excluded in the OBE solved here. The correct description of optical transitions pumped by spectrally broad pulses requires the consideration of the detuning between the field and the transition energy and the integration of the pulse spectrum [183]. However, a non-resonance enters the OBE as

additional dephasing term, which speeds up the dephasing. The time-shift between the rate equation model and the OBE would therefore be smaller when considering the detuning [183, 189].

Another simplification of the OBE defined in Eq. 4.10-4.14 is that only electronic states are incorporated, nuclear degrees of freedom are neglected. When considering vibronic states, pump and probe pulses also might generate vibrational coherence between two vibrational levels of one electronic state (ground or excited state) [102]. This coherence might cause stimulated Raman scattering contributions to the pump-probe signal. These contributions have the opposite sign of an absorption signal, which is not observed in the experiment. This is not surprising due to the large energy difference compared to vibrational energies between the pump and the probe pulse of about 5500 cm^{-1}.

Finally, it should be noted that the OBE, the calculated signals, and the discussion above are explicitly oriented to the cation absorption as the probe transition. The temporal shifts induced by the coherence however will depend on the chosen transition. This should be taken into account, especially if ultrashort time constants are extracted from transient differences of several electronic transitions within a rate equation model [21].

4.1.1.4 Data fitting - coherent contributions to the pump-probe signal

In the section above the effect of coherences to the pump-probe signal has been discussed in the limit of sequential contributions, i.e. the system interacts twice with the pump field and subsequently with the probe. As first discussed by Boyd and Mukamel [198] in the situation of temporal overlap of pump and probe pulses the ordering of the interactions with the fields may be mixed, which gives rise to coherent contributions [154, 155] (also called "coherent spike" or "coherent artifact"). As these non-resonant effects superimpose the early sequential pump-probe signal [199, 101] they can cause erroneous conclusions if pump-probe transients are incautiously interpreted as the time-dependence of populations.

It is intuitive to separate contributions from the glass substrate together with the TiO_2 film from contributions emerging from the dye, as this separation can be realized in experiment. Non-resonant electronic coherences arising from the glass substrate or the unsensitized TiO_2 film have been reduced to below 10^{-4} transmission change by minimizing the interaction area of pump and probe pulses by using a thin glass substrate (see section 3.2.2.3). This has been checked by measuring unsensitized samples. The absence of solvent is of great advantage in that context, as this usually is the main source of coherent contributions.
Stimulated Raman scattering might also contribute with mixed field order. But as

for the sequential term this effect is significant only for pump and probe pulses being spectrally near.
Finally, multi-photon absorption pathways should be considered. Multi-photon excitation of perylene has been investigated in several studies (see Ref. [200] and references therein). The existence of a S_n state between 37000 and 38000 cm^{-1} above S_0 accessible via 2-photon absorption has been reported by different authors. The next higher state is assumed to be at around 45000 cm^{-1}. The sum of the energies of pump (435 nm) and probe (570 nm) pulses is about 40500 cm^{-1}. Thus, incidentally this combination of pump and probe wavelength does not match a possible 2-photon transition. Multi-photon excitation will not significantly contribute to the pump-(cation)-probe signals.

In summary, as a good approximation the pump-probe signal of the perylene cation absorption can be interpreted as the cation population, even on the ultrafast time scale within overlapping pump and probe pulses. Thus, the pump-probe signal directly reflects the build-up of the product of the ET process. It should be noted that these are characteristic features of the perylene chromophore and can not be transferred to other systems.

4.1.1.5 Determination of the system function

The extraction of electron transfer times requires a reliable determination of the cross-correlation (CC) of the pump and the probe pulses. The CCs mostly were taken as 2-photon induced photoconductivity in SiC diodes [114]. The reliability of this method has been studied by Lochbrunner *et al.* and found to be superior to SHG-CC measurements [115].

The long-term stability of the laser system with respect to the pulse durations was found to be excellent. For example, the transient absorption shown in Fig. 4.1 was averaged for roughly 2 hours. The CCs taken before and after the transient absorption measurement almost coincide and the Gauss-fits of the CCs have both a FWHM between 27 and 28 fs. In general, fitting the CCs with Gauss-functions resulted in better fits compared to $sech^2(t)$-shaped functions.

4.1.2 ET mechanism

Now we can turn back to the discussion of the electron injection process itself. The rise of the cation absorption shown in Fig. 4.1 reveals a time constant below 15 fs. However, as pointed out in section 1.2.2, the high rate of the heterogeneous ET is no proof for an adiabatic process. A crucial point for the understanding of the ET process is the nature of the photoexcited state.

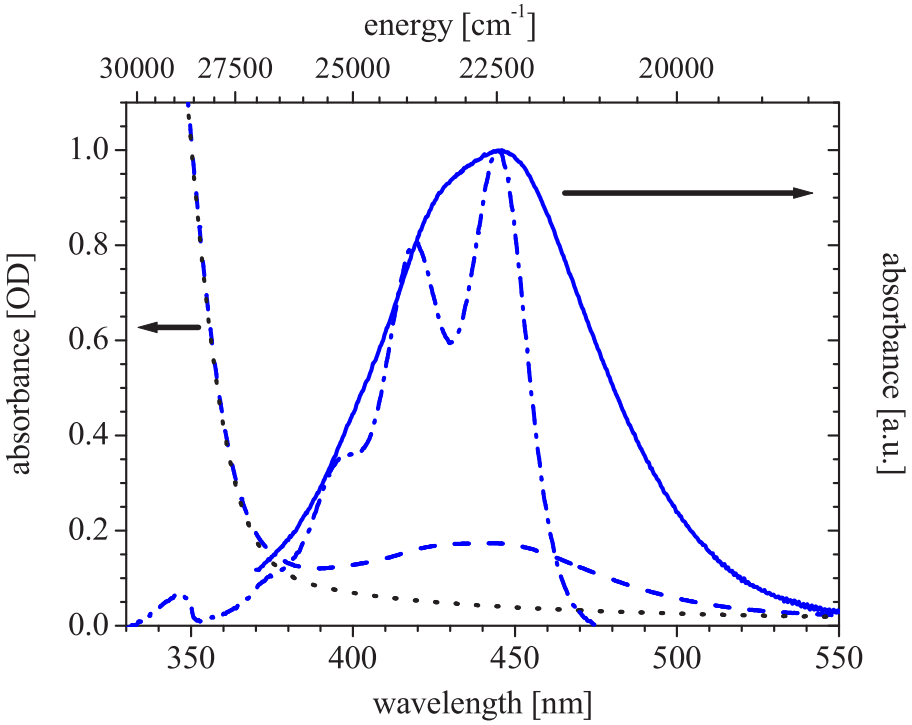

Figure 4.7: Absorption spectrum of sensitized (dashed line) and unsensitized (dotted line) TiO_2 films. The normalized difference spectrum (solid line) is shown in comparison to the normalized absorption spectrum of DTB-Pe-COOH in 1:1 toluene/methanol (dash-dotted line).

4.1.2.1 Stationary absorption spectroscopy

The stationary absorption spectra of the adsorbed dye in comparison with the free molecule provide some information on the disturbance of the molecular excited state by the conduction band states. This is shown in Fig. 4.7. The free dye in solution shows the characteristic Franck-Condon spectrum of perylene (dash-dotted line). The wavefunctions of HOMO and LUMO/excited state of this dye are shown in Fig. 3.5, visualizing a slight shift of electronic density toward the anchor group induced by the optical transition. However, this intramolecular charge rearrangement does not alter the absorption spectrum significantly compared to unsubstituted perylene.

The situation is different for the dye on the anatase surface: the Franck-Condon progression of the net dye absorption (solid line) in the sensitized film is almost washed out, the absorption band is significantly broadened with a tail on the red edge of the absorption band, and the center of the band is red shifted by about 600 cm^{-1} (75 meV).
There can be two sources for changes in the absorption spectrum. Firstly, the strong electronic coupling induces a mixing of the molecular state with the semiconductor

states, resulting in several mixed states with a certain spread of the energy eigenvalues around the energy of the undisturbed molecular state. The spread reflects the strength of the electronic interaction and, if interpreted as lifetime broadening, also the injection time. If the molecular state couples to a homogeneous continuum with a constant density of states (DOS) the spread of mixed states will be symmetric around the initial state.
Secondly, spectral changes might indicate contributions from so-called charge transfer (CT) transitions. CT absorption has been observed for various homogeneous [201, 202, 203] and heterogeneous [89, 204, 90, 205] ET systems. To which extent the optical transition directly transfers population is highly system dependent. A pure CT transition is equivalent to a direct photoinjection process. This CT transitions may arise as new absorption bands. An example therefore is catechol linked to anatase [206, 207, 76]. Although free catechol in solution does not show any absorption above 300 nm catechol-sensitized anatase obeys an absorption band above the absorption threshold of anatase. Persson and co-workers investigated this system computationally and identified the CT band as a direct catechol $\pi \rightarrow$ *conduction band* transition [76]. The appearance of such a new band in the absorption spectrum can be considered as the extreme case, where no molecular orbitals are involved in the photoexcited state. The oscillator strength of a CT transition should be highly sensitive to the spatial overlap of ground and photoexcited state, and thus will strongly depend on the spatial extension of bulk states and the presence of surface states or surface resonances. Therefore CT transitions appear not necessarily close to intramolecular transitions in the absorption spectrum.

In the case of DTB-Pe-COOH the broadened absorption band is surely no *pure* CT band as it spectrally close to the molecular absorption[3]. Additionally, the shoulder at 435 nm for the adsorbed dye gives a hint to the presence of molecular Franck-Condon progression. Fig. 4.1.2.1 shows the net dye absorption for both cases fitted with a minimal set of peak functions (Voigt functions). It is obvious to fit the spectrum of the free dye with four peaks. If the Gauss-Lorentz-ratio within each Voigt function is allowed to be a free parameter, the fit converges with strong Gaussian character (about 90%) of all peak functions. The spectrum of the adsorbed dye could also be fitted with four Voigt functions, however due to lack of structure the fit does not converge unambiguously. Therefore a minimum number of parameters was used to reproduce the spectrum: the relative positions of the three peaks used were kept fixed at the values of the free dye. With this constraint the spectrum below 26000 cm^{-1} cannot sufficiently be fitted, in particular the red tail of the band. This indicates that the shape of the spectrum arises not only by peak broadening. Allowing the outer two peaks to be asymmetric reproduces the spectrum with the minimum nuber

[3]For comparison: for alizarin-sensitized anatase the maximum of the absorption band shifts by 2750 cm^{-1} with respect to the unbound dye [90, 89].

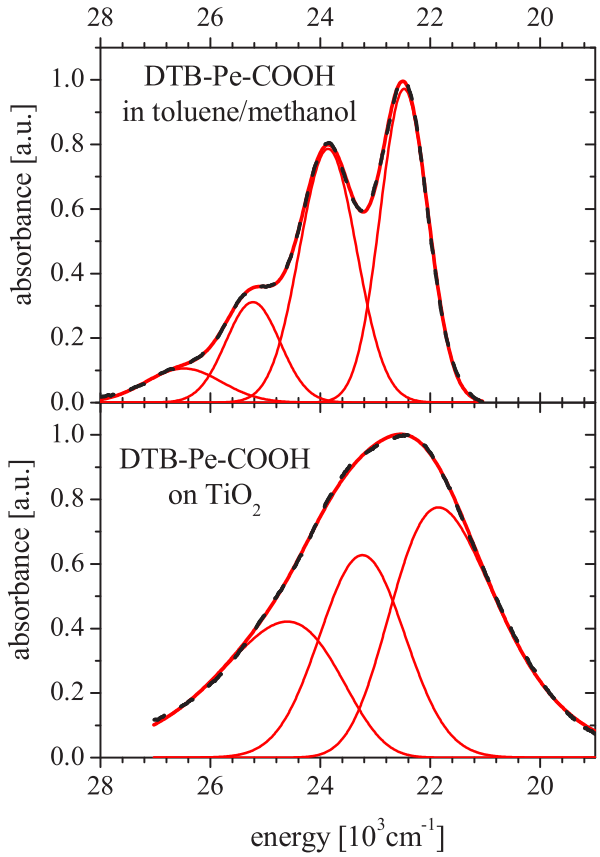

Figure 4.8: Normalized net dye absorbance (black dashed line) for free and adsorbed DTB-Pe-COOH and the appropriate fits (red solid line). Upper panel: the spectrum in toluene/methanol (1:1) is fitted with four Voigt peaks at 22480 cm^{-1} (FWHM: 1020 cm^{-1}), 23860 (1220), 25230 (1160), and 26480 (1620). Lower panel: with fixed relative peak positions the center of gravity of the absorption band shifts by 600 cm^{-1} to lower energy. The outer peaks are allowed to be asymmetric, the FWHM of the center peak increases to 1820 cm^{-1}.

of parameters. But there is no physical reason for asymmetric lineshapes, which indicates that there are additional contributions from CT transitions. Wheather these contributions are spread all over the absorption band or they mainly constitute the red tail of the band cannot be concluded from the blurred spectrum. Also the origin of the broadening, which might be homogeneous lifetime broadening or inhomogeneous broadening due to a distribution of different binding sites, can not be concluded.

Although the lower spectrum does not allow a quantitative analysis some qualitative conclusions can be drawn:

- The binding of the molecule to the surface significantly alters the dye absorption spectrum. This changes can be ascribed to the excited state rather than to the HOMO[4]. Therefore the system can be considered to be in the **adiabatic limit**.

- The remaining signature of the molecular absorption spectrum as well as the

[4]The HOMO is energetically located in the band gap of anatase, wherefore the interaction should be much weaker. Secondly, considering the MOs of the free molecule in Fig. 3.5, the HOMO is less extended toward the anchor group compared to the excited state, what additionally reduces the coupling.

small spectral shift of the band indicates that **the photoexcited state prevailingly is a local excited molecular state**. This is strongly supported by the intermediate excited state absorption signal (Fig. 4.2), which would be absent for a direct photoinjection.

- The red tail of the absorption band might arise from **CT contributions**. This would imply that the overall ET rate increases with red-tuning of the pump pulse. This has not been checked above 450 nm. Variation of the pump pulse spectrum between 425 and 450 nm (the range where sufficient short laser pulses were achieved) does not show significant changes of the ET kinetics.

4.1.2.2 Electronic structure calculation of the dye-anatase system

The electronic interaction disturbs the linear absorption spectrum. But from the spectral changes no quantitative conclusions regarding the distortion of the excited state can be drawn. To gather microscopic insight theoretical approaches are therefore highly desirable. The required size of the system however is computationally demanding. P. Persson and co-workers investigated different adsorbates on anatase and rutile surfaces on a semi-empirical level within a cluster calculation approach [75, 76, 77, 78]. As pointed out by these authors the density of states of the solid and thus the size of the TiO_2 cluster is essential for a correct description of the adsorbate-semiconductor interaction. If the level spacing in the conduction band is too large, the interaction with the adsorbate becomes arbitrarily dependent on incidental level matching of the molecular state with a particular conduction band level. Persson *et al.* also investigated pure TiO_2 clusters on the *ab initio* level and optimized the geometric structure of cluster with up to 38 (TiO_2) units [209].

Recently, P. Persson and M. Lundqvist investigated the perylene chromophore linked via different bridge-anchor groups to a DFT geometry optimized $(TiO_2)_{60}$ cluster [208]. The model system for Pe-COOH is shown in the left of Fig. 4.9. The chromophore is assumed to bind dissociatively in a bi-dentate bridging manner, the dissociated hydrogen is included in the system and forms a hydroxyl group with an adjacent surface oxygen. The DFT cluster calculation reveals the time-independent eigenfunctions and the appropriate eigenvalues. The resulting total DOS is shown in the upper panel of Fig. 4.9, together with the projected density of states (PDOS) of the adsorbate. In comparison with the level alignment obtained by UPS and XPS (section 3.4) the calculation gives a realistic description of the system. The molecular HOMO is located in the lower half of the band gap. As no excitations are calculated the LUMO is interpreted as excited state. For semi-empirical calculations of the free perylene this was justified with respect to the wavefunction, but not for the eigenvalue (section 3.1, Ref. [122]). The DFT cluster calculation reveals the

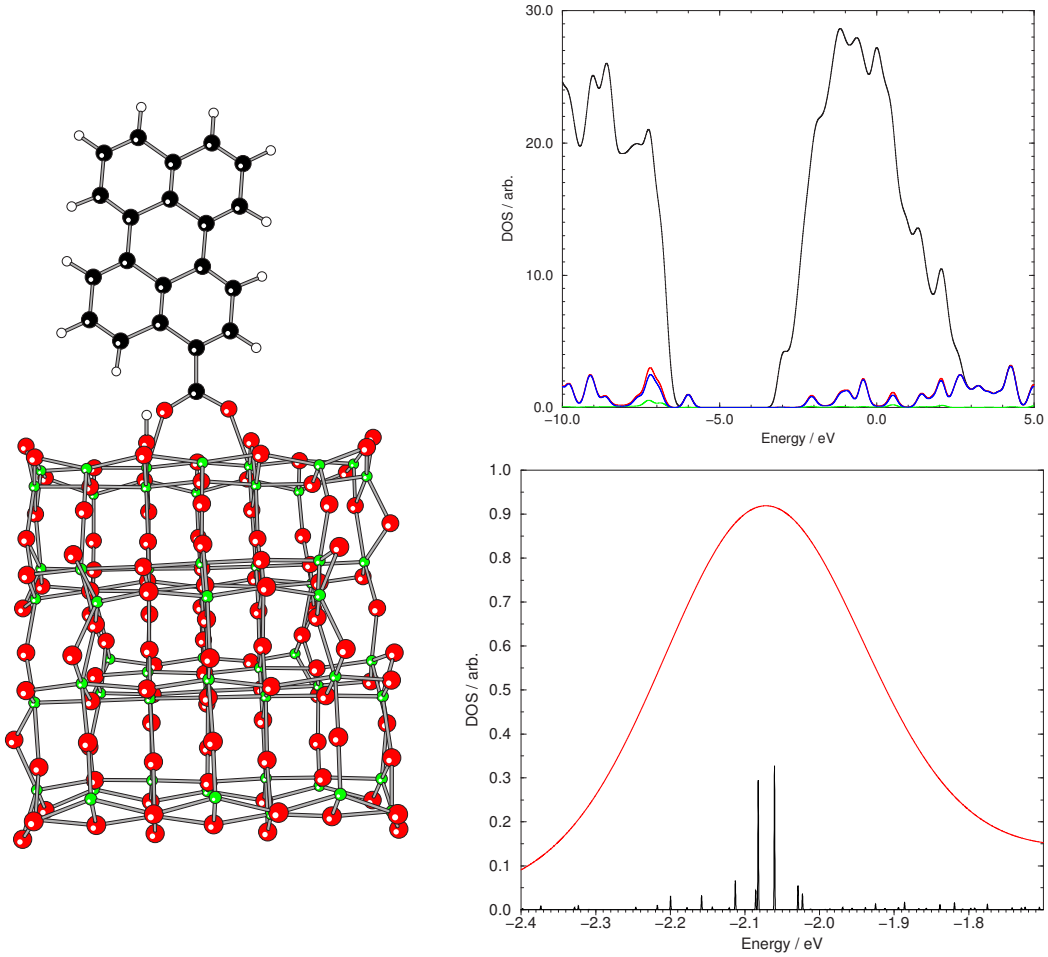

Figure 4.9: Left: Pe-COOH adsorbed on a geometry optimized $(TiO_2)_{60}$ cluster. Right, upper panel: total DOS (black line), PDOS of the adsorbate (red line), PDOS of the perylene backbone (blue line), and PDOS of the anchor unit (green line). Lower panel: PDOS of the adsorbate in the range of the LUMO (black sticks). The red line is a convolution of the stick spectrum with a Lorentzian. Results of Persson and Lundqvist [208].

LUMO energy slightly more than 1 eV above the CBM, which is in good agreement with 0.8-0.9 eV estimated from UPS and linear absorption. Thus, with respect to the level alignment the LUMO is a good substitution for the excited state.

Although this approach is purely stationary and does not provide a time-dependent description of the ET process, the excited state lifetime and thus the injection time can be indirectly deduced. In section 1.2.2 it has been argued that electronic interaction might affect a mixing of molecular and semiconductor states. This is the case in the calculated system. The lower panel on the right hand side in Fig. 4.9 shows a section of the projected density of states ($PDOS_{dye}$) on the dye, which might be expressed in term of the projected charge density $\rho_{dye,n}$ of a particular eigenfunction

Ψ_n with eigenvalue E_n on the dye,

$$\mathrm{PDOS_{dye}(E)} = \delta_{\mathrm{E,E_n}} \sum_{\mathrm{n}} \rho_{\mathrm{dye,n}} = \delta_{\mathrm{E,E_n}} \sum_{\mathrm{n}} \int_{\mathrm{dye}} |\Psi_{\mathrm{n}}(\mathrm{r})|^2 \,\mathrm{dr} \,. \tag{4.17}$$

δ_{E,E_n} denotes the Kronecker delta function, and the index "dye" at the integration indicates a restriction to the space occupied by the adsorbate. Without any coupling the $\mathrm{PDOS_{dye}}$ in the range of the molecular LUMO consists of one single stick only with $\rho_{\mathrm{dye,LUMO}}= 1$. The $\mathrm{PDOS_{dye}}$ of the adsorbed dye, however, shows several states with significant localization on the adsorbate. The summation over $\mathrm{PDOS_{dye}}$ in the vicinity of the LUMO again results in 1. From the spread of $\mathrm{PDOS_{dye}}$ an effective level broadening Γ can be defined as the occupation-weighted root-mean-squared deviation of the eigenvalues from the average energy:

$$\Gamma = \int \mathrm{PDOS_{dye}(E)} \sqrt{(\mathrm{E} - \mathrm{E_0})^2} \,\mathrm{dE} = \sum_{\mathrm{n}} \rho_{\mathrm{dye,n}}, \sqrt{(\mathrm{E_n} - \mathrm{E_0})^2} \tag{4.18}$$

which results in 99 meV. Interpreting this as lifetime broadening indicates an injection time of $\tau = \hbar/\Gamma = 6.7$ fs. This is a factor of two faster than the experimental value.

It should be remarked that a single mixed eigenstate obtained from the cluster calculation can not be considered as photoexcited state for itself. The oscillator strength of a transition from a localized molecular state to such a partially delocalized, mixed state will arise from local (intramolecular) dipole moments. In a graphical description: the transition will transfer population from one state to the other spatially localized within or close to the dye. The course of the excitation and rapid dephasing will alter the electronic structure, in particular the wavefunction of the excited state itself. Additionally, for excitation with a spectrally broad field several wavefunctions are involved, and an electronic wavepacket is formed. Thus it is unlikely that the stationary wavefunctions of the unexcited system reflect the extension of the excited state immediately after excitation. A time-dependent theory could provide such information.

In section 4.3 experimental and theoretical values for another two chromophores are discussed. At this point it should be noticed that the lifetime deduced from line broadening and the experimental value are in the same order of magnitude.

4.1.2.3 Energetics of the ET reaction

From stationary photoelectron spectroscopy and linear absorption the position of the photoexcited state can be estimated to about 800 meV above the CBM (see section 3.4). The second important quantity is the reorganization energy of the ET

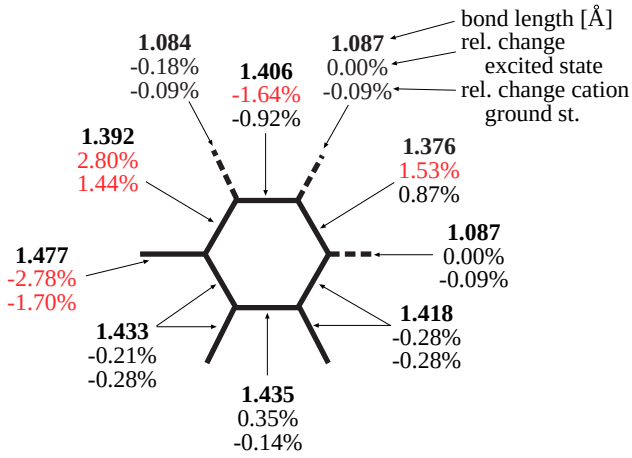

Figure 4.10: DFT-optimized geometries (B3-LYP, basis set: 6-31G(d)) of perylene in the neutral ground state S_0. The image shows the irreducible part of the molecule with D_{2h} symmetry. C-C and C-H bonds are indicated as solid and dashed lines, respectively. The upper values give the bond length in Å. The relative geometrical changes for the first excited singlet state S_1 and the cation ground state D_0 are given as middle and lower value, respectively. See text for details. Results from P. Persson and M. Lundqvist [208].

process. The intramolecular contribution to the total reorganization is a measure for the vibrational energy of the molecular product of the ET.

For free molecules the reorganization energy of excited states can be estimated from the Stokes shift of the fluorescence spectrum. But the fluorescence of the adsorbed dye is very effectively quenched by the ultrafast electron injection. Anyway, as ET occurs significantly faster than vibrational relaxation, a time-dependent method is required. Resonance Raman spectroscopy in combination with the time-dependent wavepacket propagation analysis could provide quantitative information on the reorganization energy [90], however such measurements have not yet been performed for the perylene system.

S. Ramakrishna, F. Willig and V. May investigated theoretically the ET dynamics of molecular state with one vibrational degree of freedom coupled to a continuum of acceptor states in several publications [70, 71, 72, 73, 74]. The investigated system, however, is a model system and does not reflect microscopic properties of the perylene-anatase system.

Microscopic information on the intramolecular energetics can be obtained from MO calculations of the pure chromophore. First, we ignore vibrational excitation of the molecule in the different states. Persson and Lundqvist performed DFT calculations of pure perylene [208]. Fig. 4.10 shows optimized geometry obtained with the 6-31G(d) basis set and the B3-LYP combination potential for the neutral molecule (D_{2h} symmetry) in the ground state. With the same method also the geometries of the molecule in the first excited singlet state S_1 and the cation ground state D_0 were calculated. These geometries are given as relative changes in Fig. 4.10. Changes of more than 1% are marked red. Both states relax very similary, but with the

S_1 state showing stronger relaxation[5]. This allows a single reaction coordinate to be defined for all the states to a very good level of approximation (accounting for about 98% of the structural relaxation effects) [208]. Along this coordinate the cation geometry is at 59% between the ground state (0%) and the excited state (100%). Table 4.1 additionally gives the reorganization energies λ with respect to the ground

state	λ [meV / cm^{-1}]	relaxation [%]
perylene S_0	0	0
perylene S_1	180 / 1450	100
Pe-cation D_0	50 / 400	59

Table 4.1: Intramolecular reorganization energies λ of perylene S_1 and cation ground state with respect to the neutral ground state.

state geometry. From these values the intramolecular reorganization energy of the ET reaction can be estimated to 180-50 = 130 meV, and the overall intramolecular reorganization (photoexcitation and ET) to 180+130 = 310 meV. Thus, *the electron injection from perylene to anatase occurs in the "wide band limit".*

Besides assuring that the wide band limit is fulfilled, the DFT results shown in Tab. 4.1 imply another interesting feature of the perylene system. From the reorganization energy and the structural parameter a rough estimation of the PES can be obtained, which is illustrated in Fig. 4.11. As no other information is available, it is assumed that both S_1- and D_0-PES are harmonic and, furthermore, have the same curvature. The x-axis reflects the common relaxation coordinate of excited state (red parabola, minimum at 100%) and cation ground state (blue parabolas, minimum at 59%). The black dashed PES reflects the horizontal position of the ground state PES (minimum at 0), but the true ground state PES is situated energetically lower by the excitation energy. The arrow indicates the optical transition onto the S_1-PES at the geometry of the ground state. The curvature of the PES has been choosen such that the reorganization energy of the excited state is 180 meV, or, in other words, such that the red parabola intersects the black dashed PES at the zero-point of the coordinate. The thick blue parabola reflects the cation ground state with the (x,y)-position defined by its reorganization and reorganization (Tab. 4.1), and the curvature adopted from the S_1-parabola. At the zero-point of the coordinate the cation potential is only 13 meV above the intersection of the others, what

[5]This behaviour can be understood qualitatively just by considering the squared wavefunctions of the different states. Looking at Fig.6 and Fig.7 in Ref. [122] it becomes obvious that the bond length changes significantly where the charge density changes between the states. For a particular bond, reduction of the charge density increases the bond length, and *vice versa*. For the cationic state both α and β wavefunctions (Fig.7) have to be considered. As the wavefunction of $(D_0)_\alpha$ is similar to S_0, and $(D_0)_\beta$ similar to S_1, the geometry of the cation state is in-between the ground and excited state structure.

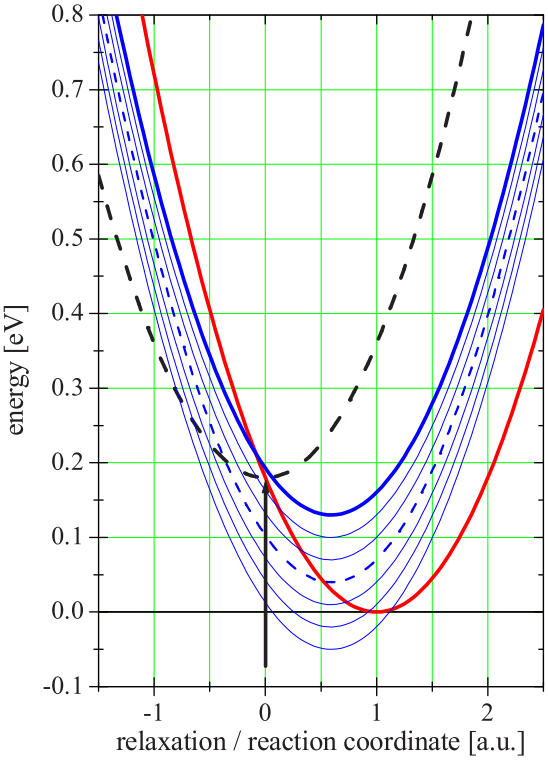

Figure 4.11: Illustration of the perylene potential energy surfaces (PES) according to the parameters from Table 4.1 with the assumption of identical harmonic potentials. The red parabola reflects the S_1 state, the black dashed PES reflects the ground state shifted vertically by the excitation energy. The cation is indicated as manifold of blue parabolas (equivalent to the illustration in Fig. 1.2). It should noted that the parabolas for each state reflect the electronic potential energy surface and not a particular vibrational eigenstate of the molecule.

indicates that the assumtions are not far off. It should be noted, that the PES in Fig. 4.11 denote the total energy of the molecule in the particular electronic states in dependence on the relaxation coordinate, but not a vibrational eigenstate of the molecule.
Now, an instantaneous excitation may excite the system according to the indicated arrow (we still ignore higher vibrational excitation). The molecule then starts moving along the S_1-PES. Due to the continuum of electronic acceptor states provided by the conduction band, ET may occur at any position of the relaxation/reaction coordinate. This is indicated by the other blue parabolas, analogue to Fig. 1.2 shown in the introduction.

The relative positions of the PES suggest an interesting implication for ultrafast injection: if the ET takes place before the molecule reaches the minimum of the S_1-PES for the first time, the injection occurs at a nuclear configuration close to the minimum of the cation PES. Such a situation is indicated as blue dashed parabola in Fig. 4.11. For this particular electron transfer pathway the overall molecular reorganization is only the 50 meV reorganization of the cation with respect to the ground state. Therefore, ET in this early time window should, in comparison with slower ET, result in molecular products with less vibrational energy. It should be

noted, that this implication follows from microscopic properties of perylene and can not be generalized to other sensitizers.

The studies of S. Ramakrishna *et al.* based on the assumption that the displacement between cation and ground state is larger compared to the displacement of the excited state. The situation outlined in Fig. 4.11 might be an interesting problem for future studies.

4.1.3 General features of pump-probe transients

4.1.3.1 Variation of pump spectrum and probe wavelength

The transient cation absorption has been measured with pump pulses at different center frequencies in the range 425 to 450 nm. The ET kinetics do not show a significant dependence. This can be explained is view of the wide band limit. Additional vibrational excitation does not gain a higher Franck-Condon-weighted density of states, as even the vibrational ground state is high above the conduction band minimum. The situation is different for adsorbates with an excited state close to the band edge [210, 175].

The observed ET kinetics also appear to be independent of the probe wavelength within the cation absorption band. Time traces taken spectrally resolved between 550 and 585 nm as well as the spectrally integrated signal do not reveal systematically varying kinetics with respect to the probe wavelength[6]. This result is somewhat astonishing. Although the unusual arrangement of the different PES might result in a relatively low vibrational excitation of the product (as discussed above), it is unlikely that the ET leads to the vibrational ground state. Therefore one would expect some evolution of the cation absorption arising from vibrational cooling, similar to the spectral evolution of the excited state absorption and the stimulated emission band for non-reacting dyes in solution [40]. However, there is a principle difference between the relaxation of an neutral molecule in the excited state and the relaxation of an ion in the ground state. A cation is an open-shell system due to the odd number of electrons. The absorption spectrum arises from contributions from both, α and β, electron spaces [122]. The relaxation process minimizes the total energy of the cation. However, it is not known clear how this affects the electronic structure in both electron spaces. Semi-empirical single point calculations, that means calculations at a fixed geometry, reveal that the HOMO-LUMO separation for the cation

[6] In the situation of not ideally compressed probe pulses the time traces at different spectral positions are slightly shifted against each other, which reflects the chirp of the probe pulses. However, the obtained rise times show the same spread as the comparison of different measurements at the same spectral position. This statement holds for all investigated dyes besides DTB-Pe-tripod.

in both electron spaces is *larger* for the relaxed geometry compared to the geometry of the neutral molecule. Unfortunately, the used software package is not capable to calculate the CI eigenstates in an open-shell system, which provide informations on the true absorption spectrum rather than the HOMO-LUMO separation. However, if the trend is correct predicted by the HOMO-LUMO separation the relaxation of the cation results in a blue-shift (!) of the absorption band. To the best of my knowledge, up to now there is no study addressing this question. A CI-calculation of the evolution of the cation absorption band along the relaxation coordinate would be highly interesting.

Directly related to the above discussion is the question if there is an oscillatory signature from a vibrational wavepacket in the cation. Zimmermann *et al.* observed an oscillatory feature in the cation signal of DTB-Pe-CH_2-P(O)$(OH)_2$ lasting up to 700 fs [19]. In this study, all five dyes besides DTB-Pe-tripod did not show an observable oscillatory signature in the cation absorption. To ensure that the pump pulse creates a coherent vibrational superposition a control measurement on the free dye in solution (tetra-tertiary-butyl-perylene in toluene) was performed. The stimulated emission signal showed an oscillatory signature with an Fourier spectrum similar to the published data [19].
There is a difference in the preparation procedure of the samples investigated in Ref. [19] and within this thesis. During the temperature-treatment of the colloidal films, alkali atoms, mainly sodium, diffuse from the glass into the nano-structured film. The presence of sodium weakens the electronic coupling of the adsorbate to the semiconductor, most likely due to changes in the binding of the molecules. This effect is discussed in section 4.4.2. The stronger electronic coupling might be accompanied by a stronger vibrational anharmonic coupling giving rise to faster vibrational dephasing. This possible relation between electronic and vibrational coupling is an interesting problem in itself. First steps in this direction were undertaken by the defined addition of sodium in the preparation procedure (section4.4.2). However, the investigation of this aspect is not yet completed. This work addresses the mechanism itself of the interfacial ET on the molecular level. Thereupon the influence of vibrational coherence on the ET can be investigated.

4.1.3.2 Photo-stability of the samples.

The experiments were performed with resting samples, i.e. all transients are taken as average of multiple scans on the same spot. This is possible due to the good photo-stability of the system under UHV conditions. Illumination of the samples with the pump pulse[7] in lab ambient results in a continuous bleach of the signal,

[7]The average pump power in the spot corresponds to the 400-fold spectrum-integrated power of the solar spectrum.

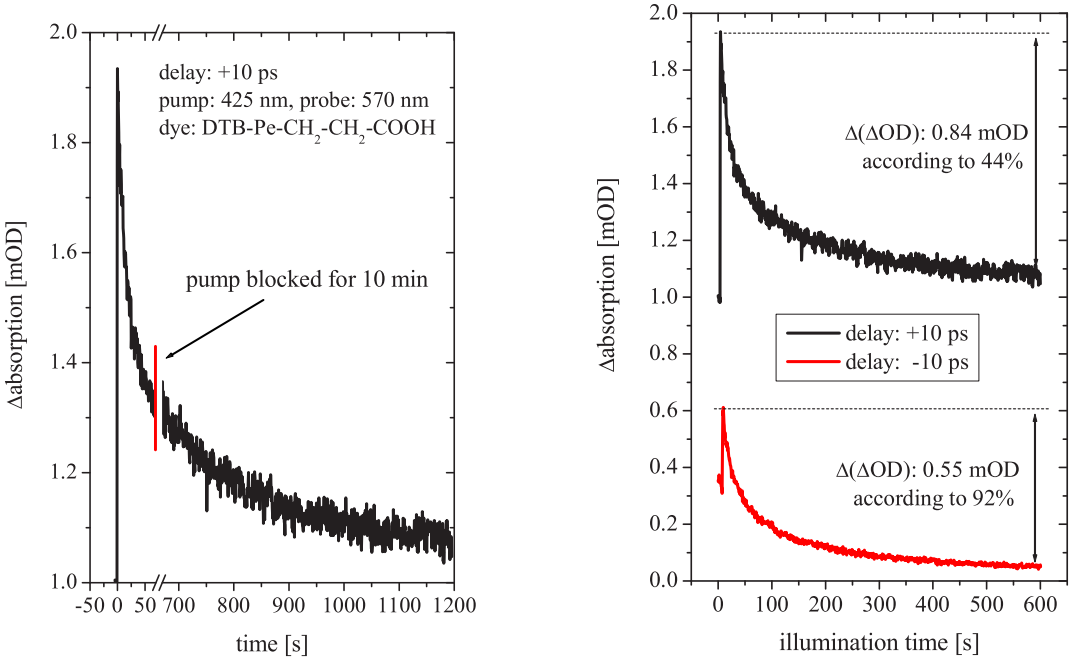

Figure 4.12: Kinetics of the initial signal bleach. Left panel: transient cation absorption at 10 ps pump-probe delay. The sample was highly dye-loaded and measured shortly after UHV conditions have been reached. This are conditions that result in a large signal loss. At t=0 the sample was moved to a new spot. The pump-probe signal immediately decreases. At t=70 s the pump beam was blocked, and unblocked at 670 s. Right panel: bleaching kinetics at +10 ps (black line, same as shown in the left panel) and at -10 ps (red line).

which is most likely caused by reaction of the cation with water [156].

In UHV the samples only show an initial bleach. The cation signals reduce by 10-50% of the initial value within about 10 min. After this initial bleach the signal stays constant within about 10% for hours. Data collection was started after the initial bleach for all transients shown in this work.

The loss of pump-probe signal is unambiguously induced by the pump pulse and does not recover with blocked pump pulse. Fig. 4.12 shows the kinetics of the bleach, i.e. the temporal evolution of the transient absorption signal at fixed delay (+10 ps) and probe wavelength (570 nm), exemplary for the cation absorption of DTB-Pe-CH_2-CH_2-COOH. During the bleach the pump beam was blocked for 10 min. After unblocking the signal continues bleaching without bend in the temporal profile (see for comparison black line in the right panel, which shows the same data without the temporal break).

Interestingly, the kinetics of the bleach is highly homogeneous within a particular

sample and at given pump intensity. However, the kinetics as well as the magnitude of the bleach for different samples vary and seem to depend on several parameters. Qualitatively, the bleach is stronger for higher dye coverage and for shorter duration of stay of the samples in UHV prior to measurement. The pump pulse intensity seems to affect only the kinetics of the bleach, but not the magnitude. Heating the samples in UHV with a halogen spotlight to 100-120 °C prior to measurement reduces the bleach during the pump-probe measurement significantly. These dependencies suggest that the bleach arises from loosely bound or unbound (physisorbed instead of chemisorbed) molecules, which desorbe photo- or thermally induced. Due to the UHV environment desorption is irreversible as soon as the adsorbate has left the sponge-like anatase film. The fact that long-term storage of samples in UHV at room temperature reduces the bleach suggests that thermal desorption is more likely than photodesorption.

In contrast to the bleach kinetics, the electron injection kinetics shows good reproducibility for equivalent samples. From the spread of time constants the error of a single measurement can be estimated to be about 20%. For comparison, the spread for differents spot on one sample is less than 5%.
Thus, the illumination of the sample prior to the start of the measurement can be regarded a "preparation" step, which removes weakly or unbound adsorbates and thus reduces the inhomogeneity with respect to the adsorbate-surface binding. The right panel in Fig. 4.12 strengthens this hypothesis. The red line shows the bleaching kinetics again taken at 570 nm, but for negative delay (-10 ps). Signal before time-zero arises from previous pump pulses. The experiments are performed at repetition rates of 100 and 150 kHz, corresponding to pulse separations of 10 and 6.67 μs, respectively. Obviously the dye cation population is not reduced completely by recombination within this time window.

The data shown in Fig. 4.12 was taken at 100 kHz. Pump-probe signal at negative delay corresponds therefore to $\sum_{n=1}^{N} I_{pp}(t_d = n \times 10\mu s)$ [8]. The bleach at negative delay in Fig. 4.12 shows a similar temporal evolution as the black line. However, the relative signal loss in terms of the initial value is 92% compared to 44%. This shows that the bleaching signal arises from dye species which obey slower recombination kinetics. That supports the assumption of a weaker surface binding of the lost species.

[8] Due to its low intensity the probe pulse does not significantly alter the cation population. An excited cation is probably reduced by hole transfer/electron capture, as the hole can be estimated to be resonant with the anatase valence band, and the lifetime of the cation excited state of perylene is in the tens of picosecond range [191].

4.1.3.3 Long-term cation signal

Figs. 4.2 and 4.12 indicate that the recombination kinetics are highly nonlinear. On the one hand, the transient cation absorption shows already within the first picosecond a significant decrease of the cation absorption signal, which can be assigned to a fast recombination mechanism with a time constant τ_{rec} of about 300 fs. On the other hand, there is still remaining transient cation absorption after 10 μs, i.e. about eight orders of magnitude later. The recombination kinetics therefore likely depend on several processes occurring on very different time scales. Section 4.4.1 provides a more detailed discussion.

The accessible time window of a fs-pump-probe experiment is limited to about 2 ns by the scan range of standard delay stages, and thus can not cover the whole time range of the recombination. At this point only the effect of slow recombination on the measurement of the forward injection shall be considered. If the system does not fully recover within the pulse separation of the laser system, the experimenter has to take care not to measure a specific subunit of the investigated ensemble. Let us assume the two borderline cases: first, the slow recombination arises only from slow electronic processes in the semiconductor. In this situation all dye molecules are approximately equivalent and the probability not to recombine within 10 μs is the same for the whole ensemble. The pump-probe experiment thus measures the average value of the system. The second limit is that the slow recombination in the range of the pulse separation is a molecular property of a subunit of the molecules. Thus only this subset would not recover due to a weaker coupling, and its influence on the fast kinetics would be underestimated. In the following sections it is shown that injection and recombination dynamics correlate. Therefore it is highly unlikely that the underrated subset would obey faster forward injection. An underestimated slower injection component only might superimpose the kinetics of the fast species and eventually alter the early recombination kinetics.
In conclusion, both limits as well as any intermediate situation will not falsify the ET kinetics of the majority of the system.

4.2 Electron transfer: Dependence on the chemical nature of the anchor group

The binding of molecules to surfaces is not only an essential ingredient in dye-sensitized solar cells. Also most scenarios for molecular electronic devices contain this building block [24]. The anchor group provides a covalent linkage of the adsorbate to the surface. The nature of this chemisorption will determine the binding strength. With respect to electronic processes, however, the strength of the *elec-*

tronic interaction mediated by the anchor is of interest. So far, this aspect has not been investigated for heterogeneous systems[9]. In the introduction and the previous section it is elucidated that the kinetics of heterogeneous ET reflect the electronic coupling strength to a good approximation.
The carboxylate group is mostly used as anchor unit for the chemisorption of molecules on semiconductor surfaces. In this section the electron injection from DTB-Pe-COOH is compared to the perylene analog linked via the phosphonic acid group (DTB-Pe-P(O)$(OH)_2$).

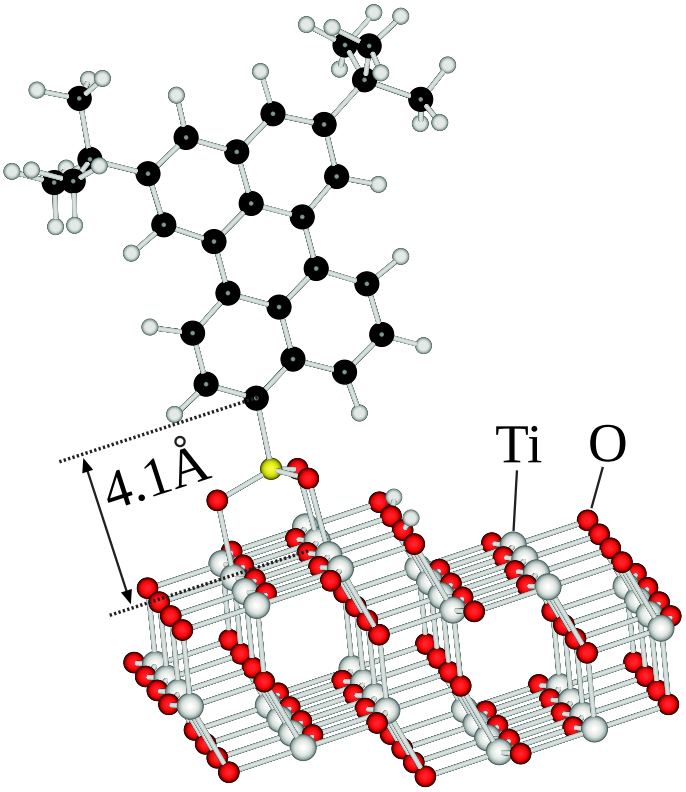

Figure 4.13: Geometry of the tri-dentate bonding of DTB-Pe-P(O)$(OH)_2$ on a $Ti_{40}O_{80}$ anatase cluster with (101) surface. The molecular structure is optimized with a molecular mechanics (MM) calculation (with MM+ force field). The geometry of the cluster was frozen at the bulk structure. The distance between the chromophore and the surface, defined as the distance between the perylene-carbon bound to the phosphorous and the surface plane, defined by the three binding titanium atoms, is 4.1 Å. The image also shows the step-like morphology of this surface.

4.2.1 Binding modes of the anchor groups

In section 3.3 the binding mode of carboxylic acids was investigated with FT-IR spectroscopy. It was reasoned that the acidic groups bind in a bi-dentate bridging fashion to the surface. Most likely two configurations exhibiting this binding character coexist: dissociative bi-dentate bridging and molecular adsorption with hydrogen bonding.
The tri-dentate nature of the phosphonate group gives rise to multiple bonding possibilities. Guerrero and co-workers proposed the tri-dentate bonding to be the most

[9]Grätzel and co-workers studied different metalorganic phosphonic acid dyes adsorbed on anatase with laser flash photolysis [211]. Due to the lack of time-resolution, the electron injection was not resolved.

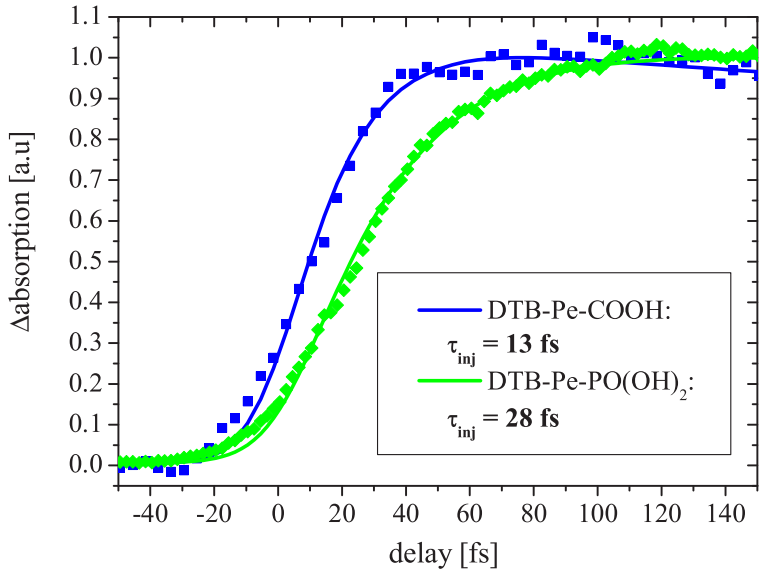

Figure 4.14: Rise of the cation absorption of DTB-Pe-P(O)$(OH)_2$ (green diamonds) adsorbed on anatase in comparison with the data from Fig. 4.1 (DTB-Pe-COOH, blue squares) after excitation with a 15 fs pump pulse (probe wavelength: 565 nm). The signal offset at negative delay is subtracted and the data is normalized. Data fitting according to Eq. 4.8 reveals injection times of 28 fs and 13 fs, respectively. Both data sets were recorded successively with the same experimental time-resolution and can directly be compared.

likely bonding mode, according to FT-IR and NMR spectroscopy of phenylphosphonic acid on colloidal anatase [212]. Additionally, these authors suggested a bidentade configuration which has a bridging geometry with a remaining OH group at the phosphorous. Fig. 4.2 shows the geometry of the tri-dentate bonding geometry obtained from a molecular mechanics cluster calculation (with MM+ force field). The distance between the chromophore and the surface is 4.1 Å. The tridentate bonding results in a vertical arrangement relative to the local surface plane with respect to the orientation of the attached chromophore relative to the surface. However, the ideal anatase (101) surface exhibits a step-like structure. Therefore, the chromophore is tilted relative to the macroscopic surface by about 20°. The bi-dentate bonding geometry is less defined. The level of interaction between the proton of the phosphonate OH group and a surface oxygen is likely to affect the configuration. Furthermore, the orientation of the dye relative to the macroscopic surface plane and thus its distance is not clearly defined due to the morphology of the local surface. A MM optimized geometry of the bi-dentate configuration is shown in the appendix (Fig. A.3). This geometry exhibits a molecule-surface distance of 4.25 Å. Analogue molecular mechanics calculations have been performed

for DTB-Pe-COOH on the same cluster (also shown in Fig. A.3). The bi-dentate bridging configuration reveals a distance of 4.0 Å, which almost equals the distance provided by the tri-dentate bonded phosphonic acid.

Pawsey *et al.* studied self-assembled monolayers of carboxyalkylphosphonic acids on colloidal TiO_2 [213, 214]. This bi-acids are saturated hydrocarbon chains with a carboxylic group and a phosphonic group on the different ends. These authors observe the bi-acids binding to the surface with the phosphonic acid anchor rather than with the carboxylic group.

4.2.2 Injection kinetics and linear absorption

The kinetics of the electron injection from DTB-Pe-P(O)$(OH)_2$ into anatase are shown in Fig. 4.14 in comparison to the perylene analog linked via a carboxylic group (same data as shown in Fig. 4.1). The phosphonic acid injects significantly slower. Both data sets were taken successively with the same experimental system function and can therefore be directly compared. Data fitting with the rate equation model reveals twice the time constant for the phosphonic anchor (τ_{inj} = 28 fs) compared to the carboxylic acid (τ_{inj} = 13 fs)[10]. The signal offset at negative delay is subtracted and the data is normalized for a better comparison. The absolute values of the offset-corrected absorbance changes are 1.0 mOD (phosphonic) and 2.0 mOD (carbonic).
The fit with a single exponential injection time reproduces the pump-probe signals remarkably well. But this should not be interpreted as an indicator of a high homogeneity of the sample. The integration over an inhomogeneous distribution of injection times can also result in a mono-exponential rise as long as the distribution is somehow peak-shaped. From that perspective, the mono-exponential rise excludes the presence of two or more binding modes with distinct, but different injection kinetics.

Let us recall Eq. 1.2: the electron injection time constant only depends on the electronic coupling and the Franck-Condon-weighted density of states. According to the UPS and XPS measurements the HOMO levels of both dyes are equally aligned with respect to the semiconductor states. As the positions of both absorption bands are close together, the *FCWD* for the injection of both dyes is essentially the same[11].

[10]The pump-probe signals are fitted by minimizing the mean square deviation of the model function convoluted with the experimental cross-correlation by using a Simplex-Downhill algorithm [215].

[11]If the red-shift of 600 cm^{-1} (75 meV) in the adsorption band of DTB-Pe-COOH has any influence, it would decrease the *FCWD* for this dye as the DOS of semiconductor states increases with energy at the position of the injection level (see top panel in Fig. 4.9).

Thus, the factor of two in the injection times reflects the difference in the electronic coupling.

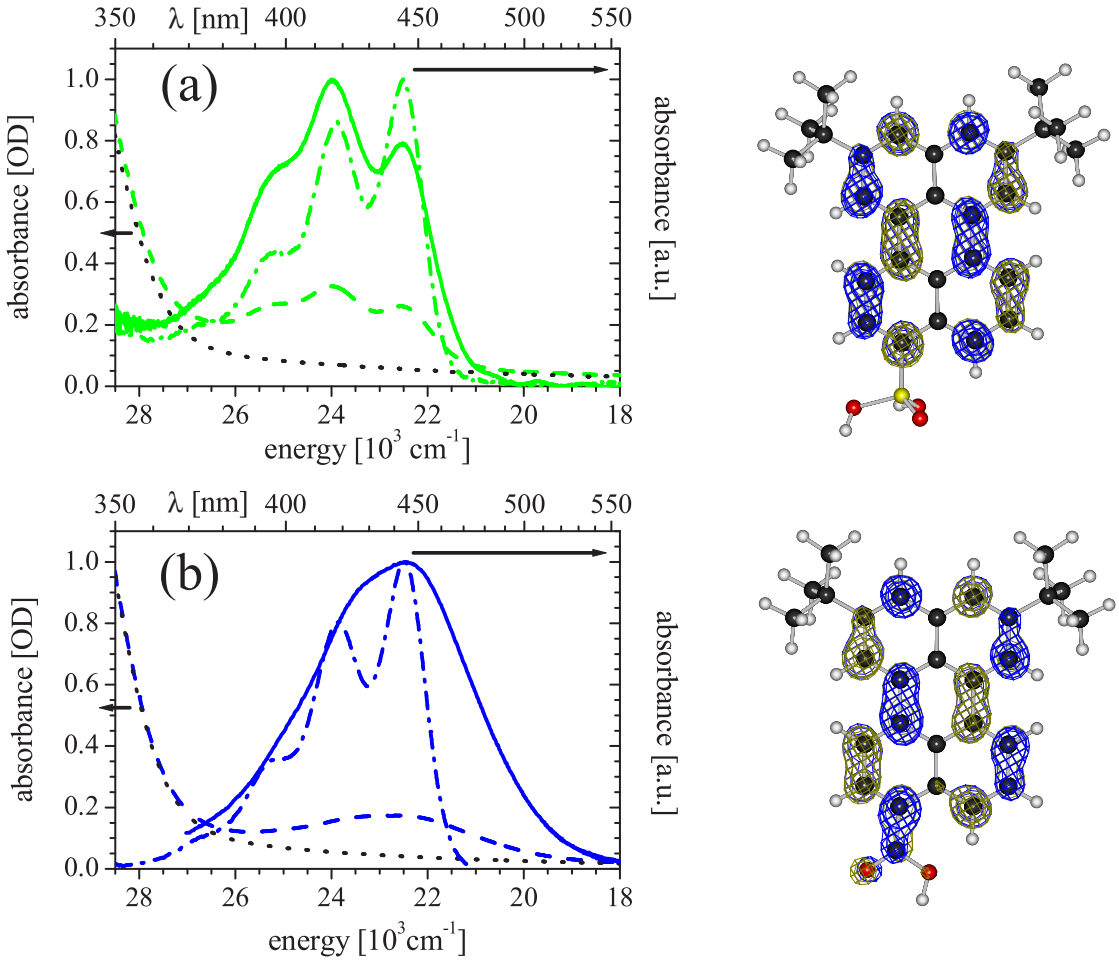

Figure 4.15: Left: Absorption spectra of DTB-Pe-P(O)$(OH)_2$ (a) and DTB-Pe-COOH (b, same as Fig. 4.7). The absorption in solution (dash-dotted lines, solvent: 1:1 toluene/methanol) is compared to the normalized net dye absorbance (solid lines) of the sensitized anatase films. The non-normalized absorbance of the sensitized and the pure films are given as dashed and dotted lines, respectively. Right: LUMOs of DTB-Pe-P(O)$(OH)_2$ (top) and DTB-Pe-COOH (bottom) calculated with PM3.

It is interesting to consider the linear absorption spectra for both dyes. Graph (a) in Fig. 4.15 shows the net dye absorption of free and adsorbed DTB-Pe-P(O)$(OH)_2$. Graph (b) shows the spectra of Fig. 4.7 for comparison. The change in the absorption spectrum induced by the adsorption is significantly different for the two dyes. The shape of the absorption spectrum of DTB-Pe-P(O)$(OH)_2$ is still clearly changed by the adsorption, but the position of the absorption band remains unchanged (multi-peak fits of both spectra reveal a marginal red-shift of about 30 cm^{-1}). The changes manifest in the peak amplitudes and the peak width of the Franck-Condon progression. The observed broadening must be partially caused by lifetime broadening. A

lifetime of 28 fs corresponds to a homogeneous line width of 190 cm^{-1} (23.5 meV). However, the multi-peak fits of the spectra result in non-uniform broadening of the individual peaks. As in the case of DTB-Pe-COOH, inhomogeneous broadening covers the lifetime broadening. Nevertheless, the absorption spectra reflect qualitatively the weaker electronic coupling mediated by the phosphonic acid anchor compared to the carboxylic group.

4.2.3 MO calculations of the anchor group

Let us now consider the origin of the weaker electronic coupling provided by the phosphonate group. Although the adsorbate-surface bonding is not unambiguously characterized for both acids, it is unlikely that geometrical effects account for the observed difference. If the number of covalent adsorbate-surface bonds would be a criteria for the mediated interaction, DTB-Pe-P(O)$(OH)_2$ would show faster injection: the number of bonds for the most likely configurations is either three or two (plus eventually a hydrogen-bond) for the phosphonic anchor, and two or one plus hydrogen-bond for the carboxylic group.
According to the molecular mechanics calculations, also the difference in the spacial separation of the chromophore from the surface is astonishing small for both anchors.

On the right of Fig. 4.15 the LUMOs of both dyes are plotted[12]. In the case of DTB-Pe-COOH, the LUMO wavefunction extends stronger into the anchor group. Quantitatively, the analysis of the wavefunctions for both molecules reveals that the LUMO is localized by 3.81% in the carboxylate group and only by 0.37% in the phosphonate group. The phosphonate group confines the wavefunction more to the perylene backbone. A graphical explanation for this behavior might be the different local geometry within the anchor group. The LUMO wavefunction of perylene has strong p_z-character (z is the axis normal to the perylene plane). As the chromophore itself, the carboxylic group has sp^2 character, which favors the interaction for states with π^* character [134]. Thus, the wavefunction strongly exceeds into the anchor (3.47% of the total anchor-contribution (3.81%) arise from the p_z-atomic orbitals of COO). In contrast, the phosphonate group exhibits sp^3-character around the phosphorus. Therefore, the LUMO exceeds as far as the P-p_z atomic orbital (0.14%), but not significantly further.

In contrast to the geometrical considerations, also the energetic position of unoccupied bridge states might be a determining factor with respect to the electronic

[12]In contrast to the previous calculations these are performed with the PM3 parametrization as the phosphorus is not incorporated in ZINDO/S. Again the LUMOs reflect the excited states in good approximation.

interaction. This aspect is the basis of the so-called superexchange mechanism of ET [57, 216]. Superexchange interaction can be simplified imagined as the electronic coupling mediated by one or several off-resonant unoccupied electronic levels between the donor and the acceptor state. The coupling strength depends on the degree of off-resonance.
In the perylene system unoccupied bridge states might mediate the electronic coupling. According to semi-empirical calculations (ZINDO and PM3) of the pure acid groups both formic acid (HCOOH) and phosphoric acid ($HP(O)(OH)_2$) have very similar, negative electron affinity (EA). That means that the pure unoccupied bridge states are at least 4 eV above the photoexcited state and are therefore unlikely to affect the electronic coupling.

The results of this section may be summarized as following:

- The observed difference in the electron injection kinetics reflects the difference in the electronic coupling.
- The change in the coupling strength of the chromophore linked via different anchor groups arises from the *molecular* electronic properties. The extension of the excited state into the anchor seems to be a crucial factor.
- As the ET kinetics reflects molecular properties semi-empirical MO calculations of the adsorbate provide helpful informations. Trends for the strength of the electronic interaction of the adsorbate with the surface can be estimated from the spacial extension of the wavefunctions.
- The linear absorption spectra qualitatively reflect the electronic interaction strength. Electron injection from DTB-Pe-COOH may be assigned to the adiabatic limit of ET, whereas DTB-Pe-$P(O)(OH)_2$ may be regarded as non-adiabatic.
- Electron injection from DTB-Pe-COOH and DTB-Pe-$P(O)(OH)_2$ into TiO_2 does not follow a superexchange mechanism.

4.3 Electron transfer: Dependence on the chemical nature of the bridge

This section discusses the effect of different molecular units inserted between the chromophore and the anchor group on the dynamics of the electron injection as well as the early backward electron transfer. Similar to the comparison of the two different anchor groups the observed bridge-dependence can be related to molecular properties.

4.3.1 Electronically saturated bridge units: methyl groups

The distance dependence of electronic interaction has been studied extensively for homogeneous ET systems (see for example Ref. [31] and references therein). In the case of interfacial ET, to the best of my knowledge, only T. Lian and co-workers have addressed the dependence of the ET kinetics on the insertion of bridge units. As already mentioned in section 1.3.1, these authors observed a dramatic decrease in the injection rate by a factor of 200 due to the insertion of a single CH_2 group between the carboxylic anchor groups and the Re-polypyridyl complex [80].

Fig. 4.16 shows the transient cation absorption of DTB-Pe-CH_2-CH_2-COOH and DTB-Pe-CH_2-P(O)$(OH)_2$ in comparison with the corresponding dyes without alkyl groups. There is a systematic trend in the ET injection kinetics: insertion of a single alkyl group in the case of the phosphonic acid anchor roughly doubles the ET time constant, whereas the insertion of two alkyl groups results in a deceleration by a factor of four for the carboxylic anchor. With the assumption that the variation of the anchor group itself only results in a different "offset" of the electronic coupling, a single CH_2 group can be assigned a factor of two in the reduction of the electronic coupling.
In analogy to the observations for the different anchor groups, the obvious reduction of the electronic coupling by the bridge elements should be reflected in the absorption spectra of the adsorbed dyes as well as in the extension of the LUMO wavefunctions onto the bridge-anchor group. Indeed, both of this observables behave as expected from the injection time. The right panel of Fig. 4.17 shows the net dye absorption of DTB-Pe-CH_2-CH_2-COOH in solution as well as adsorbed on anatase. In comparison with the spectra of the carboxylic acid and the phosphonic acid shown in Fig.4.15, the trend of weaker disturbance of the absorption spectrum for slower ET clearly proceeds. The absorption spectrum of the methyl-phosphonic acid is qualitatively equivalent to the propionic acid.

With respect to the electronic structure, the occupation of the LUMOs on the anchor groups (exclusive bridge) is 0.12% for the propionic and 0.06% for the methyl-

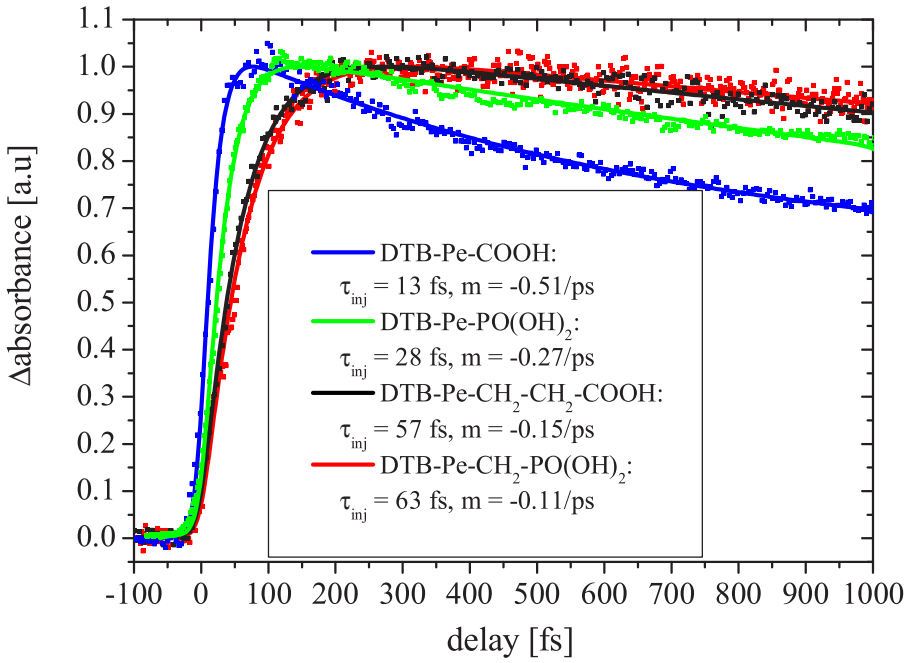

Figure 4.16: ET transfer dynamics through different saturated bridge-anchor groups: Rise of the cation absorption of DTB-Pe-CH_2-CH_2-COOH and DTB-Pe-CH_2-P(O)$(OH)_2$ in comparison with the analogous dyes without bridge units. Data fitting reveals time-constants of 57 fs for the phosphonic acid and 63 fs for the methyl-phosphonic acid, respectively. After the electron injection is completed, the cation absorption decreases due to recombination. In comparison, the recombination kinetics reflect the kinetics of the forward injection. The early decay of the cation signal has been fitted with a straight line for the time windows 100-500 fs (DTB-Pe-COOH and DTB-Pe-P(O)$(OH)_2$) and 250-1000 fs (both others). The resulting slopes are given in the inset.

phosphonic acid. The molecular geometries in these calculations are similar to the molecular structures shown in Fig. A.4. However, the extension of the wavefunctions onto the bridge-anchor unit depends on the orientation of the anchor groups relative to the perylene backbone. There is no clear energetic minimum in the semi-empirical geometry optimization procedure of these molecules. The given values provide a lower limit of the occupation of the LUMOs on the anchor and should only be regarded as rough estimates. In section 4.3.3 the mediation of electronic coupling in dependence on the electronic structure of the bridge elements is discussed in detail.

This bridge-dependence is strikingly different compared to the result of Lian and co-workers. As pointed out in section 1.3.1, this difference might arise from ultrafast intersystem crossing concuring with electron injection in the Re-complex. In such a situation the observed difference due to a bridge element reflects both, a change in the coupling strength as well as the difference in the injection time between the singlet and the triplet state. This situation does not occur for perylene, as is shown

by the long fluorescence lifetime of all derivatives (Fig. 3.6).

It should be noted that a molecular bridge consisting of alkyl groups is flexible. Therefore it is likely, that both perylene dyes, the methyl-phosphonic acid and the propionic acid, exhibit a broad distribution of bonding geometries. In the case of the propionic acid even complete back bending of the chromophore is possible. However, molecular mechanics calculations of the adsorption geometry do not show complete back bending for both anchors. The calculations converge in tilted geometries (see Fig. A.4 in the appendix). In any case the DTB groups prevent the direct contact of the perylene backbone with the surface. The minimum through-space distance is 3.4 Å for the obtained geometry, in contrast to 6.0 Å through-bridge distance.

Despite the distribution of bonding geometries, which has to be assumed, the rise of the cation absorption in Fig. 4.16 can be fitted with a single time constant for all four dyes. This behavior is reproducible for different measurements. Mathematically, the integration over a distribution of reaction rates results in a temporal evolution of the product that can be described with a stretched exponential function [217]. However, a stretched exponential dependence is similar to a mono-exponential function on the short timescale of the reaction. Nevertheless, the presence of ultrafast contributions to the overall injection rate can be excluded due to the good agreement of the data with the mono-exponential fit model.

Symmetry of forward and backward ET.
Turning back to Fig. 4.16, the decay of the cation absorption signal sets in immediately after the electron injection is completed. Interestingly, the dependence of the kinetics of this early recombination on the bridge-anchor group reflects the dependence of the electron injection. The slopes of linear fits to the early decay of the signal are given in the legend of the graph. The obtained values indicate an even qualitative symmetry between forward and backward ET. As discussed in detail above, the electron injection is determined by the electronic coupling of the excited state to the conduction band. The electron recombination is mediated by the coupling between a semiconductor state and the LUMOs of the oxidized molecule. Assuming that the character of the injected electrons does not significantly change within the first hundreds of femtoseconds (for instance by trapping), this symmetry visualizes that the electronic interactions for both directions of ET transfer are proportional to each other. This conclusion suggests that the extension of the cationic LUMOs onto the bridge anchor group is similar to that of the neutral excited state. This is the case indeed, according to the semi-empirical calculations. This aspect is discussed within the following section.

The absolute values of the transfer rates for forward and backward ET differ significantly for two reasons. First, the relative occupations of the states are very different

for both directions. In the case of the injection, a single occupied state experiences an empty continuum. In the reversed situation, an electron in a single occupied state within an otherwise empty continuum may transfer into the molecular state, but likewise also to another state in the continuum. A fully occupied continuum interacting with a single empty molecular state would truly be the inverted situation compared to the injection. This situation arises for an empty molecular state, e.g. the hole in a photoexcited molecule, which is in resonance with the valence band of the solid. Hitherto, such a "hole transfer" has not been investigated in an heterogeneous ET system. According to the symmetry evincing in Fig. 4.16, the hole transfer should occur on the same time scale as the electron injection and, additionally, should exhibit a similar dependence on the bridge-anchor group.
A second reason for the asymmetry in the injection/recombination rates is the different energetic position of the cation LUMO compared to the neutral excited state. ZINDO/S calculations (on PM3, AM1 and ZINDO/1 optimized geometries) yield LUMO eigenvalues of -5.1 eV (α) and -5.7 eV (β) relative to the vacuum level. With respect to the neutral molecule, this levels lie about 1 and 1.5 eV above the neutral HOMO, i.e. still in the band gap of the TiO_2. The Franck-Condon-weighted density of states in Eq. 1.2 is thus different for both directions of ET. For the different bridge-anchor groups, however, the *FCWD* are equivalent.

4.3.2 Electronically unsaturated bridge: DTB-Pe-CH=CH-COOH

4.3.2.1 Electron injection

Compared to sp^3-hybridized bridge units, the bridge-mediated coupling becomes essentially different for unsaturated bridge groups. Fig. 4.18 shows the rise of the cation absorption of perylene-acrylic acid (DTB-Pe-CH=CH-COOH) in comparison with the sp^3-hybridized analog propionic acid and the bridge-free carboxylic acid. Although for this dye the spacial separation of the perylene ring structure from the surface is very comparable to the case of the propionic acid, the electron injection occurs at a rate very similar to bridge-free carboxylic acid (top panel in Fig. 4.18). The fit of the transient cation absorption with the rate equation model reveals an injection time constant of 10 fs. The spread of the time constants obtained from different samples is about 20%, thus a single time-trace is not sufficient to judge about such small differences. However, several measurements confirmed this trend of a slightly faster injection from the acrylic acid.

Again, the stationary absorption spectra reflect the kinetics of the electron injection (Fig. 4.17). The absorption spectrum of adsorbed DTB-Pe-CH=CH-COOH (left panel) shows qualitatively the same features as the carboxylic acid (Fig. 4.7):

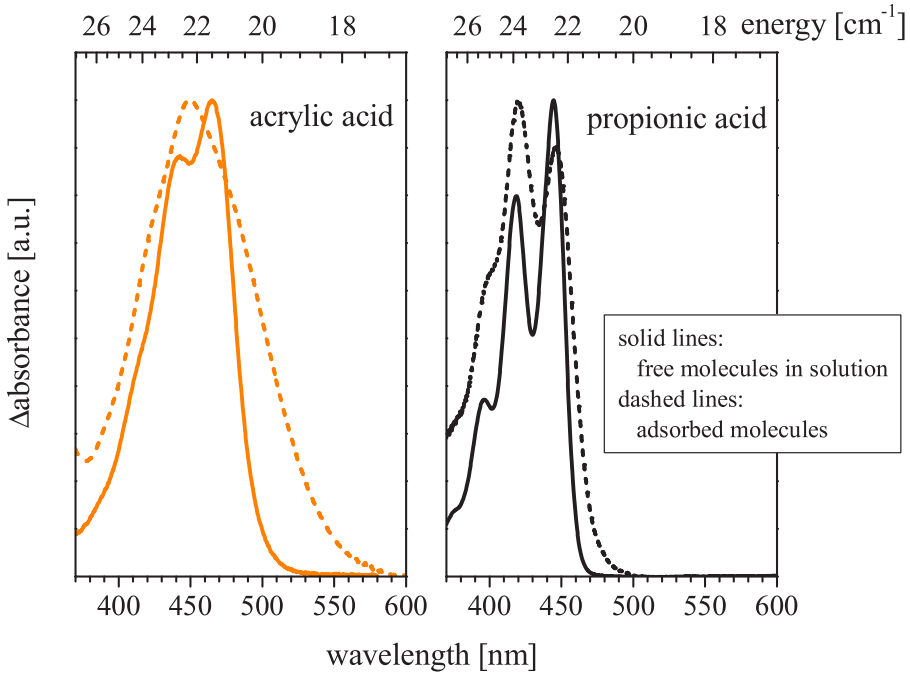

Figure 4.17: Absorption spectra of DTB-Pe-CH=CH-COOH (left panel) and DTB-Pe-CH_2-CH_2-COOH (right panel) in 1:1 toluene:methanol (solid lines) and adsorbed on TiO_2 (dashed lines).

significant broadening, a slight red-shift of the center of the band, a red tail, and a remaining signature of the Franck-Condon progression. In section 3.1 the red-shift of the free DTB-Pe-CH=CH-COOH absorption band (see Fig. 3.4) of about 1100 cm^{-1} was assigned to the extension of the excited state into the conjugated bridge. This extension is visualized in Fig. 4.19. Quantitatively, 2.4% of the acrylic acid LUMO are localized on the carboxylic group[13]. The comparison with the corresponding values of the other dyes (3.8% and 0.1%) reveals that the partial density of the excited state wavefunction on the anchor is capable to predict trends of the interfacial electronic coupling.

Photoelectron spectroscopy of the dye-anatase interface reveals no dependence of the HOMO position on the bridge-anchor group exceeding the experimental uncertainty of about 100 meV. As the excitation energy of DTB-Pe-CH=CH-COOH is lower by 140 meV, also the injection level of this dye is lower compared to both others. However, the DOS of the conduction band is increasing with higher energy at that energetic position (see top panel in Fig. 4.9). If at all, the *FCWD* for the acrylic acid should be smaller. A significant effect arising from different *FCWD* to the bridge-dependence is therefore unlikely.

[13]For comparability this value has been obtained from a PM3 calculation.

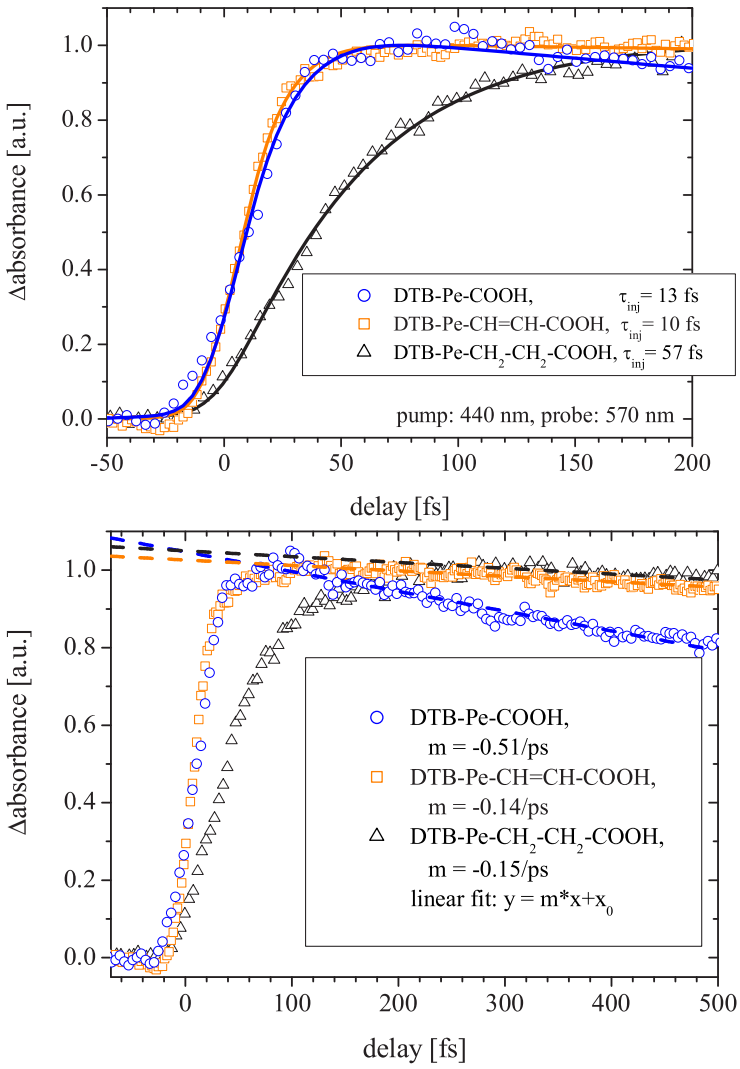

Figure 4.18: Rise and early decay of the cation absorption of DTB-Pe-CH=CH-COOH in comparison with the perylene-carbonic and -propionic acid. Top panel: The fit of the pump-probe signal according to Eq. 4.8 reveals an injection time of 10 fs for the perylene-acrylic acid, which is even slightly faster than the injection from the chromophore directly adsorbed via the carboxylic group. Lower panel: Same data for a different time range. The decay of the cation signal is fitted with a linear function. The resulting slopes are given in the inset.

4.3.2.2 Comparison with DFT cluster calculations

In section 4.1.2.2 recent results of P. Persson and M. Lundqvist obtained by DFT cluster calculations have been discussed for the perylene-carboxylic acid. These authors also studied the other two dyes shown in Fig. 4.18. The calculated splitting Γ (Eq. 4.18) of the molecular projected density of states PDOS_{dye} (Eq. 4.17) is a measure of the excited state lifetime according to $\tau_{calc} = \hbar/\Gamma$. The results are summarized in Table 4.2. The trend in the injection times for the different dyes is well demonstrated by the calculation. The absolute values for the injection time revealed by the calculation are a factor of two faster in comparison with the experimental results.

It should be noted that the calculation is purely *ab initio*. The difference in the absolute value is not surprising. There are quite a few parameters giving rise to differences from the ideal theoretical model. Some examples: different crystal surfaces of the colloids, carbon impurities on the surface, a distribution of binding geometries

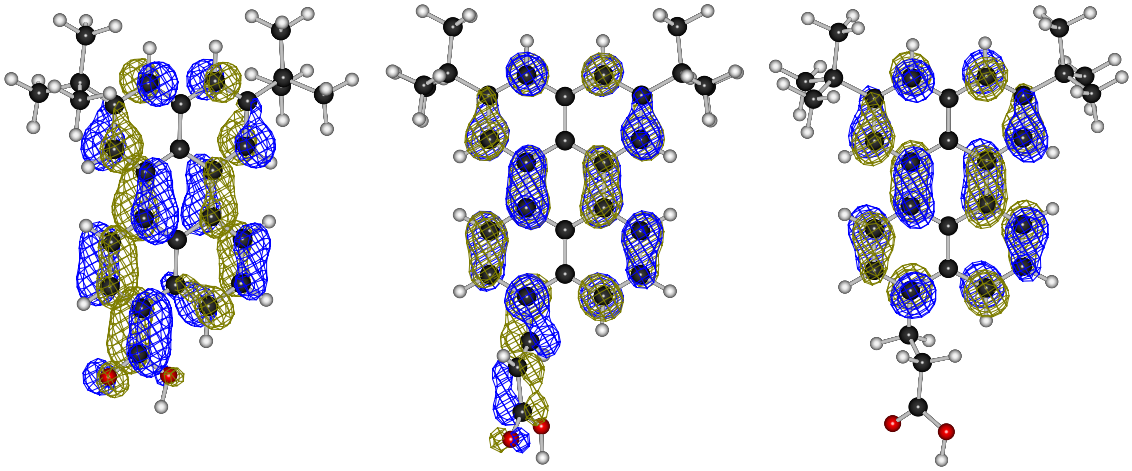

Figure 4.19: LUMOs of DTB-perylene-carbonic, -acrylic and -propionic acid (from left to right). As the perylene LUMO has pure π^* character the wavefunction extends onto the sp^2-hybridized bridge of the peryleny-acrylic acid. Wavefunctions calculated with ZINDO/S on a ZINDO/1 optimized geometry.

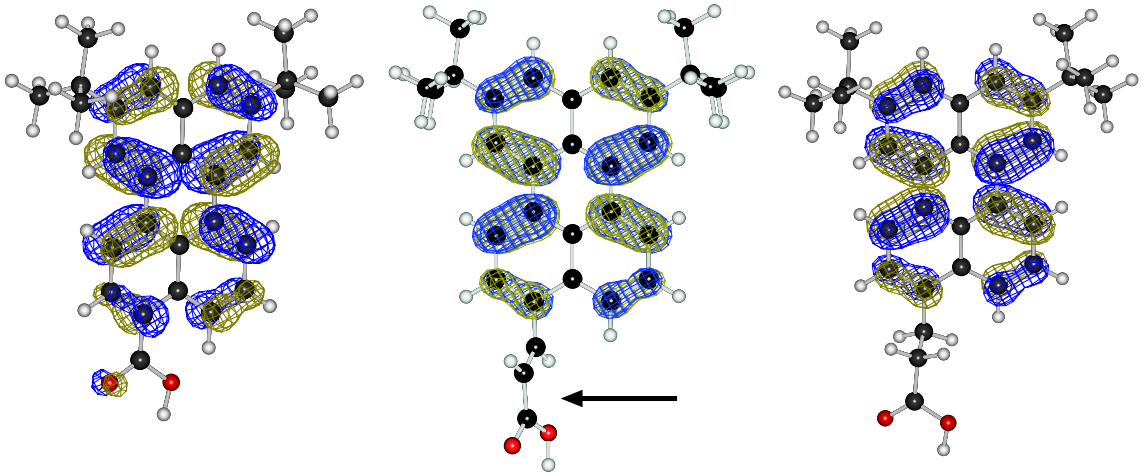

Figure 4.20: β-LUMOs of oxidized DTB-perylene-carbonic, -acrylic and -propionic acid (from left to right). In contrast to the LUMO of the neutral dye (Fig. 4.19), the conjugated bridge is not involved in the MO. The α-LUMOs behave qualitatively equivalent. The geometries are optimized by UHF-ZINDO/1 calculations.

dye	Γ [meV / cm^{-1}]	τ_{calc} [fs]	τ_{exp} [fs]
Pe-COOH	99 / 800	6.7	13
Pe-CH=CH-COOH	81 / 650	8.1	10
Pe-CH_2-CH_2-COOH	18 / 150	37	57

Table 4.2: Calculated splitting Γ of the molecular PDOS$_{dye}$ for perylene-carboxylic acid, acrylic acid, and propionic acid obtained from a DFT cluster calculation. The model consists of the chromophore bonded to a relaxed $(TiO_2)_{60}$ cluster. The theoretical electron injection time is $\tau_{calc} = \hbar/\Gamma$. See text and section 4.1.2.2 for details. Results of P. Persson and M. Lundqvist [208].

rather than the assumed dissociative bi-dentate bridging configuration, differences in the alignment of the molecular levels with respect to the semiconductor state.
In view of the inhomogeneity and the imperfection of the experimental nano-structured system, the discrepancy of the factor of two seems to be small.

4.3.2.3 Early recombination

The qualitative difference between the alkyl (sp^3) and the alkenyl (sp^2) bridge may be called insulator-like and wire-like behavior in the language of molecular electronics. For intramolecular ET these two regimes of electronic interaction have been observed in various systems. However, the time scales for homogeneous ET through "molecular insulators" [43, 46, 218] and "molecular wires" [48, 49, 50, 219] are in the picosecond to nanosecond range.
In the case of strongly coupled donor-bridge systems the differentiation of a bridge from a donor part is somewhat artificial. The LUMO of the perylene-acrylic acid incorporates the alkenyl groups equivalently to any other part of the perylene ring structure itself. With respect to the first excited singlet state, this molecule could also be seen as new chromophore (DTB-Pe-CH=CH-) directly bound to a -COOH anchor group.
However, this does not hold for other electronic states, and this is reflected by the kinetics of the early recombination shown in the lower panel of Fig. 4.18. Contrary to the symmetry between forward and backward ET observed for the sp^3-hybridized bridge-anchor groups, the acrylic acid injects as fast as DTB-Pe-COOH but recombines similar to DTB-Pe-CH_2-CH_2-COOH. The qualitative, physical explanation for this behavior is nicely given by the LUMOs of the oxidized dyes, i.e. the electronic states, which are important for the recombination. Fig. 4.20 shows the β-LUMOs of these molecules. The striking difference compared to the states of the neutral molecules (Fig. 4.19) is the missing extension onto the bridge (marked with an arrow). Expressed in the fancy language of molecular electronics, the sp^2-hybridized bridge is wire-like in one direction of ET and insulator-like in the opposite. There-

fore, *the alkenyl bridge has the character of a molecular diode* [220, 221, 222]. The α-LUMOs of the three oxidized dyes show qualitatively the same behavior.

The physical origin of the different extensions of the neutral and the cationic LUMOs arises from the different energy eigenvalues of these states. As can be seen in Figs. 3.2 and 3.7, the characters of the cationic and neutral LUMOs are very similar. However, the eigenvalue of cationic β-LUMO is about 1.5 eV below the neutral excited state according to CI calculations[14]. Separating the perylene body and the bridge in a gedankenexperiment, the perylene cation LUMO is less resonant with the bridge LUMO compared to the neutral LUMO and therefore does not mix with the bridge.

It should be remarked that it is not known if the carboxylic group of DTB-Pe-CH=CH-COOH is in *trans*- or *cis*-configuration with respect to the perylene. PM3-calculations reveal a slightly lower total energy for the *trans*-geometry (by 25 kJ/mol = 260 meV). The extension of the LUMO wavefunction onto the bridge is less pronounced for the *cis*-configuration. However, the same holds for the cationic *cis*-isomer. Therefore, the qualitative discussion above holds for both of the isomers.
Some molecules in solution show fast *cis-trans*-isomerization after photoexcitation. In principle it is possible that DTB-Pe-CH=CH-COOH also undergoes an isomerization process after electron injection, which alters the electronic coupling. This is the principle of the so-called molecular switches [223]. However, it can be ruled out that such a process occurs for DTB-Pe-CH=CH-COOH linked to the surface within the first hundreds of femtoseconds, as the process would involve in a significant motion of the whole perylene backbone.

4.3.3 Distance dependence of electronic coupling: MO study of the perylene-bridge coupling

In the discussion above, the different extension of wavefunctions onto the bridge group has been assigned to differences in the energy matching of the perylene states and the bridge states. This finding reveals that the bridge-mediated electronic coupling sensitively depends on the electronic structure of the given system. There are numerous studies on the strength and the distance dependence of electronic interaction for different bridges [43, 44, 46, 218, 45, 47, 48, 49, 50, 51, 52, 31]. Theoretical studies basing on Koopman's theorem [61] investigate the bridge-mediated coupling by the level splitting of two "probe states" (e.g. an ethylene group), which are on each side of the bridge [46, 218, 45, 47, 51]. However, there are no theoretical studies, which consider the through-bridge electronic coupling between extended π-systems

[14] In general, excited state wavefunction can not be compared to LUMOs. However, in the case of neutral as well as oxidized perylene the LUMO wavefunctions reflect the excited states remarkably well by more than 95% (see dicussion in section 3.1).

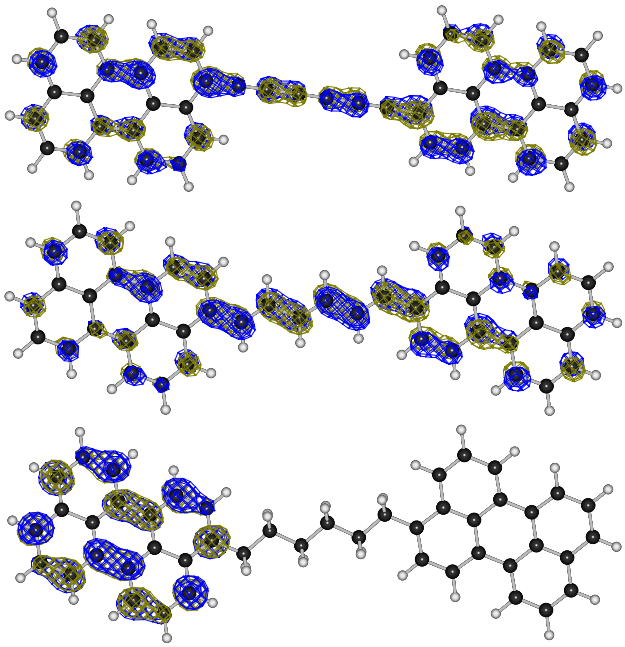

Figure 4.21: Bridge mediated electronic interaction: LUMO wavefunctions of an artificial perylene-bridge-perylene molecule with sp-hybridization (bridge: -$(C)_6$-, top), sp^2-hybridization (-$(CH)_6$-, middle), and sp^3-hybridization (-$(CH_2)_6$-, bottom). Without coupling the electronic levels in both perylene moieties are degenerate and there are two equivalent LUMOs. Electronic coupling affects a splitting of the levels by $2V_{AB}$ and causes the delocalization of the wave function over the whole molecule.
Geometry optimized with ZINDO/1, electronic structure calculated with ZINDO/S.

with a size comparable to perylene.
Therefore, MO calculations on an artificial bi-perylene molecules have been performed in order to gather some trends of the distance dependence of electronic interaction mediated by different bridge units. The considered molecules have the structure Pe-bridge-Pe with bridge elements of different length and different hybridization. As example, three molecules with six bridge elements with sp-, sp^2-, and sp^3-hybridization are shown in Fig. 4.21. In the case of the alkyl and the alkenyl bridges an all-trans configuration has been assumed. The calculations are ZINDO/S single point calculations on the ZINDO/1-optimized geometries.

It should be noted that the considered molecules are no ET systems but only used to judge on the electronic coupling from the perylene chromophore via different bridges. For that reason, no transition state has to be found, at whose geometry the splitting between donor and acceptor equals twice the coupling strength (see Fig. 1.1 for visualization). Therefore, the splitting at the relaxed geometry reflects the electronic interaction between both perylene moieties. The validity of the assignment of the HOMO splitting to the electronic coupling relevant for electron transfer is discussed for example in Ref. [46, 224, 218].

Fig. 4.21 shows the LUMOs of Pe-$(C)_6$-Pe, Pe-$(CH)_6$-Pe, and Pe-$(CH_2)_6$-Pe. The electronically unsaturated bridges mediate significant electronic interaction, which results in a mixing of the two initially degenerate LUMOs of both moieties. Thus, the LUMO and the LUMO+1 are both delocalized over the whole molecule and split with respect to their energy eigenvalues by twice the coupling. In the case

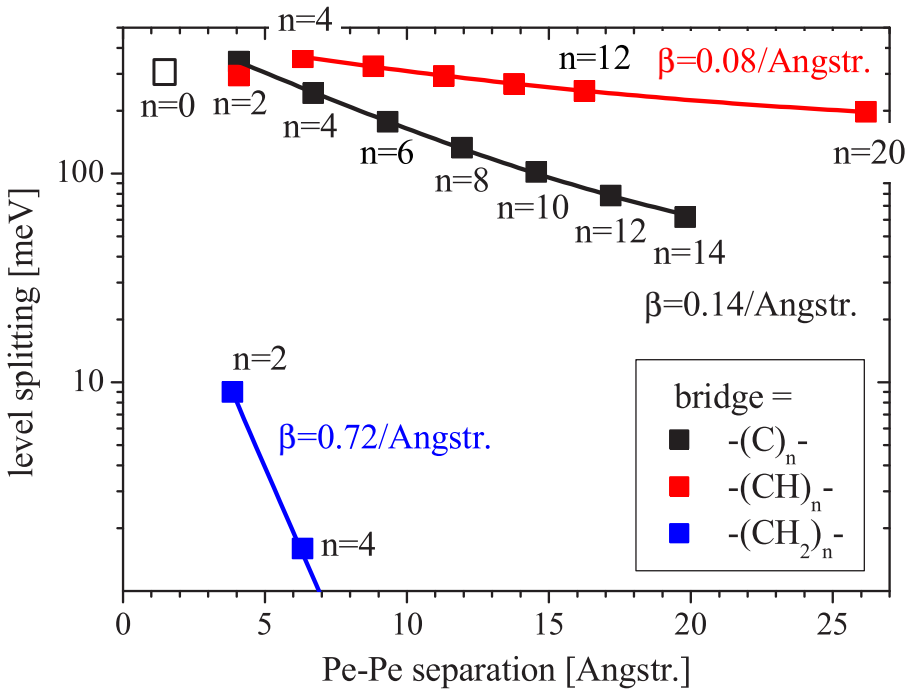

Figure 4.22: Distance dependence of electronic coupling in dependence on the chemical nature of the bridge. Energy splitting of LUMO and LUMO+1 in the symmetric perylene-bridge-perylene molecules shown in Fig. 4.21 for different bridge length.

of the saturated, sp^3-hybridized bridge, six CH_2 groups are sufficient to decouple electronically both perylene subunits. The HOMO and the HOMO+1 are therefore localized on the different moieties and degenerate in energy.

The results on the LUMO-LUMO+1 splitting in dependence on the number of bridge elements is summarized in Fig. 4.22. Interestingly, the alkenyl bridges mediate the coupling stronger as the sp-hybridized bridges and show the weakest distance dependence. The distance dependence is fitted with a mono-exponential function and the distance parameters β are given in the graph. In the case of the saturated bridge, there are only two points before the states degenerate within the semi-empirical calculations[15]. Nevertheless, the value of 0.7/Å obtained from this two points is in good agreement with published work on saturated bridges [224, 218, 31].

With respect to interfacial ET it should be noted that there are no anchor groups included in the model. Therefore, the absolute values of the coupling strength for the differently hybridized bridges can hardly be compared and put into relation with the observed differences in the electron injection time. However, the influence of the anchor groups can be assumed to be equal if only the bridge length is changed, similar to the assumption that the semiconductor DOS is a constant. Therefore, the

[15]High-level DFT calculations reveal electronic coupling through saturated bridges up to 15 Å [31].

distance dependence of electronic interaction should be reasonable predicted by the applied method.

It should be noted that the distance dependence of the electronic interaction might be significantly different if higher unoccupied states are considered. It would be interesting to apply above method on a perylene bi-cation. However, this requires UHF calculations, which should be performed with symmetry restrictions for the molecule. This is not capable within the software package used.

4.3.4 Long-range electron transfer: DTB-Pe-tripod

In the previous section, long-range electronic interaction through hydrocarbon chains is considered theoretically. In real systems, a large separation of the donor from the surface can only be achieved with rigid molecular units. Such a bridge molecule is the so-called tripod, which has been synthesized in the group of E. Galoppini, Rutgers University [85, 86]. Within a collaboration with the HMI, in particular with S. Felber, the tripod was linked with the DTB-Pe chromophore [129]. The structural formula of DTB-Pe-tripod was shown in Fig. 3.3. In terms of the chemical nature, the tripod molecule contains both saturated and conjugated bonds. The tripod consists of an adamantane ($C_{10}H_{16}$) center, which is a sp^3-hybridized molecule, and four phenyl (sp^2) substituents. Three of the phenyl arms are terminated with carboxylic groups, the fourth is linked via an acetylene group with the chromophore. Due to the sp-hybridized linker, the perylene wave functions extend onto the acetylene and to less extent also on to the phenyl ring. The LUMO of DTB-Pe-tripod is shown in Fig. 4.23. The extension of the LUMO gives rise to a red-shift of the ground state absorption by about 20 nm, similar to DTB-Pe-CH=CH-COOH (see Fig. 3.4).

The left panel of Fig. 4.23 shows the kinetics of the electron injection from this chromophore into anatase, again as the rise of the cation absorption. The rise of the product signal is clearly multi-exponential. The transient absorption can be fitted with three time constants of 30 fs (29%), 340 fs (24%), and 1950 fs (47%). Repeated measurements on identically prepared samples revealed a significantly poorer reproducibility compared to the five dyes discussed before. However, a three-exponential kinetics was observed for all measured samples. All absortion signals showed a fast component of about 30 fs, an intermediate time constant between 300 and 700 fs, and a long time constant between 1.9 and 4.5 ps. The minimal and maximal relative amplitudes of each time constant in each data set are about 25% and 50%, respectively.

The most prominent differences of DTB-Pe-tripod compared to the other perylene derivatives are its size and the number of anchor groups. Both features may give rise to a higher inhomogeneity of the system. The intention of a large donor-acceptor

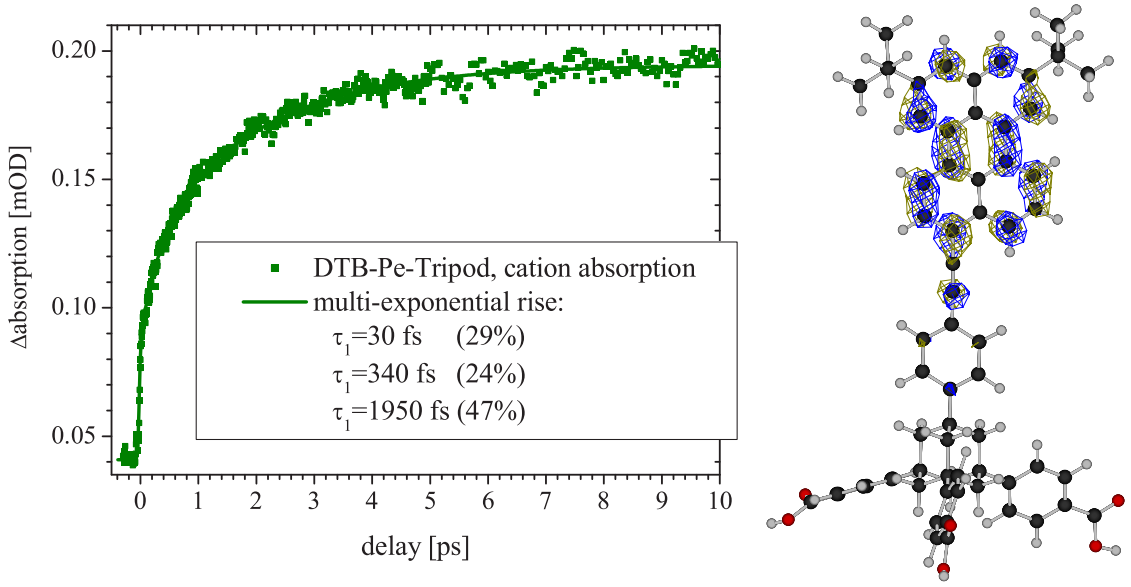

Figure 4.23: Left panel: Electron injection from DTB-Pe-tripod into TiO_2 probed as the rise of the cation absorption at 590 nm. Right: The LUMO of DTB-Pe-tripod extends onto the acetylene group. The distance between the acetylene group and the surface is about 10 Å if all three carboxylate groups bind to the surface.

distance is only realized if all three anchor groups actually bind to the surface. With only two binding anchors the molecule may actually lie flat on the colloidal surface rather than standing upright.
Additionally, the overall size of DTB-Pe-tripod is about 25 Å (carboxylic group to DTB), which has to be compared with the mean pore diameter of the porous film of 95 Å obtained from BET measurements. Thus, there is likely a significant number of binding sites, which provide a short distance of the chromophore subunit to a surface, even if all of the anchor groups bind to the surface. In view of this argumentation, the longest of the three time constants shown by each sample arises from molecules standing ideally upright.
Recently, P. Piotrowiak *et al.* studied the electron injection from Ru-tripod complexes (featuring an additional phenyl ring between chromophore and adamantane) into anatase and observed a bi-exponential kinetics with a fast time constant around 300 fs and a slow component with about 3 ps [225].

The ground state absorption and the emission spectra of DTB-Pe-tripod are red-shifted. Fig. 4.24 shows the transient cation spectrum of this dye (dark green line) in comparison with DTB-Pe-CH_2-CH_2-COOH (black line with diamonds) 100 ps after the arrival of the pump pulse. The probe pulse in this measurement was an uncompressed white-light continuum. The cation spectrum of DTB-Pe-tripod is significantly broadened and red-shifted by about 20 nm, but it exceeds the narrow absorption band of the perylene-propionic acid toward the blue as well. Therefore,

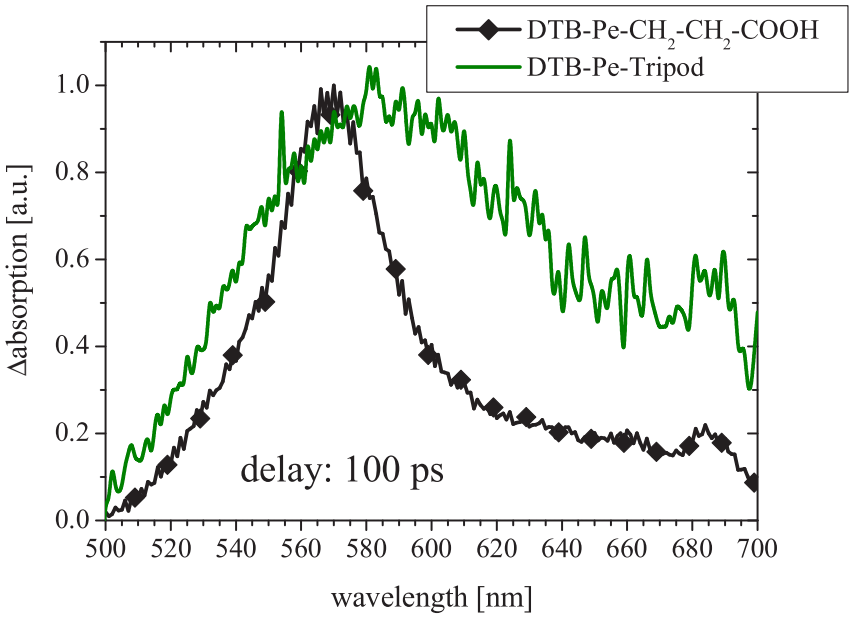

Figure 4.24: Transient absorption spectrum of DTB-Pe-tripod (dark green line) and DTB-Pe-CH_2-CH_2-COOH (black line with diamonds) adsorbed on anatase 100 ps after the arrival of the pump pulse centered around 445 nm.

the emission and the cation absorption overlap roughly between 500 and 570 nm.

Fig. 4.25 shows the transient absorption of the perylene-tripod at 550 nm. This signal is a superposition of stimulated emission (negative signal) at early delay times and the cation absorption. The data is fitted with a three-exponential rate equation model, which takes both signal sources into account. The obtained time constants are within the range mentioned above with a slowest injection time of 4.1 ps and a relative amplitude of 26%.

Within the first 500 fs the signal shows an oscillatory feature, as shown in the inset. The right panel of Fig. 4.25 shows the power spectrum of the Fourier transform of the fit residuals, which exhibits a sharp peak at 385 cm^{-1}. As discussed above (section 4.1.3), Zimmermann *et al.* observed oscillations in the transient stimulated emission of TTB-perylene in solution [19], which arise mainly from two frequencies at 360 and 420 cm^{-1}. This frequencies can be assigned to Raman-active normal modes of the perylene chromophore [19, 124]. It is likely that these modes cause the peak in the Fourier spectrum in Fig. 4.25 but are not resolved due to the fast decay of the oscillations within 500 fs.

The oscillatory feature can be ascribed to the stimulated emission contribution to the signal rather than the cation absorption. Transient absorption signals taken at shorter wavelength clearly show oscillations, whereas transient absorption signal around 600 nm are smooth, as shown in Fig. 4.23.

In recapitulation, the pump pulse creates a vibrational wave packet in the pho-

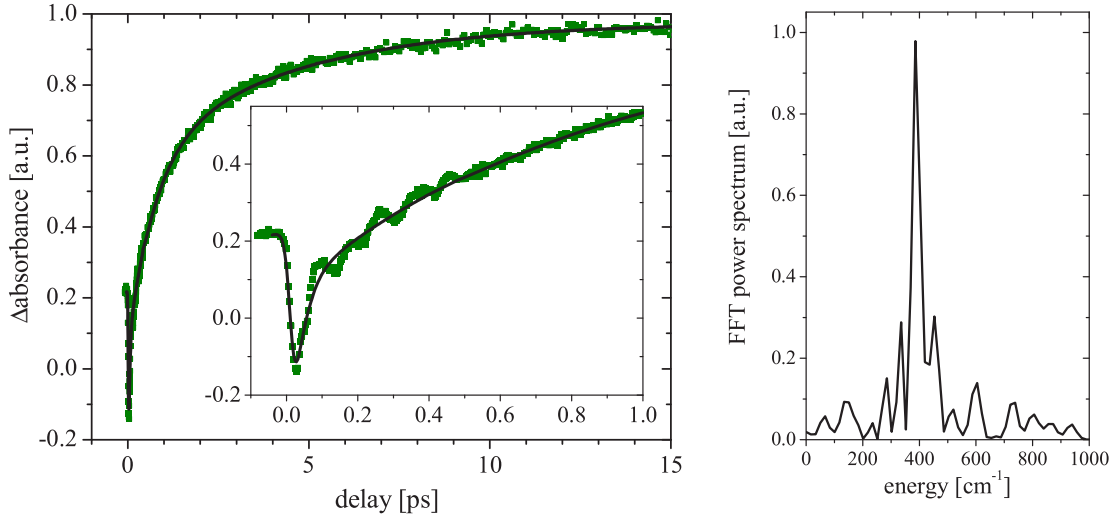

Figure 4.25: Left panel: Transient absorption of adsorbed DTB-Pe-tripod at 550 nm. The signal is a superposition of stimulated emission (negative signal) and cation absorption. The inset shows oscillatory features of the signal within the first 500 fs. Right panel: The Fourier spectrum of the fit residuals.

toexcited state of DTB-Pe-tripod. However, so far no signature of a vibrational coherence in the molecular product state of the ET has been observed. The next step will be the study of the possible influence of the wave packet in the donor state on the ET process.

4.3.5 Summary - distance dependence of electron transfer

It is interesting to compare the long-distance ET with the directly coupled chromophore DTB-Pe-COOH. If we associate the long time constant (≈3 ps) of DTB-Pe-tripod with the upright geometry, the ratio of the injection times between tripod and carboxylic acid is 230. The difference in the dye-surface distances is about 10 Å - 4 Å = 6 Å. Assuming an exponential distance dependence (Eq. 1.8), this corresponds to a distance parameter β of 0.9/Å, which is in qualitative agreement with the value obtained theoretically for the saturated bridges (Fig. 4.22) and in good agreement with the distance dependence obtained theoretically for σ-bonded rigid rods [31]. This β-parameter reflects the distance dependence of electronic coupling in the non-adiabatic limit.

The comparison of the short bridge-anchor groups reveals a systematic dependence, as discussed above. Apparently there is a factor of two reduction of the reaction rate per CH_2 group. However, it is not clear how much the distance is increased by the insertion of one CH_2 group, due to the wide spread of possible binding geometries for the flexible bridges.

In the case of both dyes directly coupled with the carboxylic and phosphonic acid anchors, the MM calculations reveal virtually the same perylene-surface distance. Thus, at the boarder between non-adiabatic and adiabatic heterogeneous ET the exponential distance dependence of the strength of the electronic interaction breaks down.

4.4 Further aspects of interfacial electron transfer

4.4.1 Recombination kinetics

Under UHV conditions, the backward transfer of an electron from the semiconductor to the oxidized molecule is the only way to reduce the molecule back to the neutral species. In the dye-sensitized solar cell the dye is reduced by an electron from the redox couple, and the recombination by an electron from the semiconductor is a loss channel.

All published transient absorption studies of the recombination revealed highly non-linear kinetics for different dyes on nano-structured anatase [13, 226, 15, 227, 228, 229, 160]. The recombination process of transition metal-organic dyes spans the time range from picoseconds to milliseconds [13, 226, 229]. This high non-linearity of the reaction arises from a number of sequential electronic processes within the semiconductor affecting the recombination. The recombination process has been mostly studied with time-resolved spectroscopy probing the population of the oxidized dye. However, this approach does not provide any informations on the electronic processes within the semiconductor. Fig. 4.26 provides a schematic illustration of possible recombination channels.

In the previous section (4.3) it was shown that the kinetics of the early recombination within the first picosecond can be explained in terms of the electronic coupling of the adsorbate. This implies that the injected electrons do not undergo significant changes like trapping into a localized state in this time scale. Thus, at early times the recombination might occur from injected electrons prior to or during the relaxation (channel (2) in Fig. 4.26) or from relaxed electrons at the CBM prior to trapping (3). If there are any unoccupied surface states present at the surface, a transient occupation of these might also be important (1). The relaxation and trapping of electrons has been found to occur on the hundreds of femtoseconds time scale [230, 231].

The electron is localized in a trap state after energetically reaching the CBM. Neither the energetic or the spatial distribution of this states nor the Fermi level of the colloids during the optical measurement are clarified. The UPS measurement

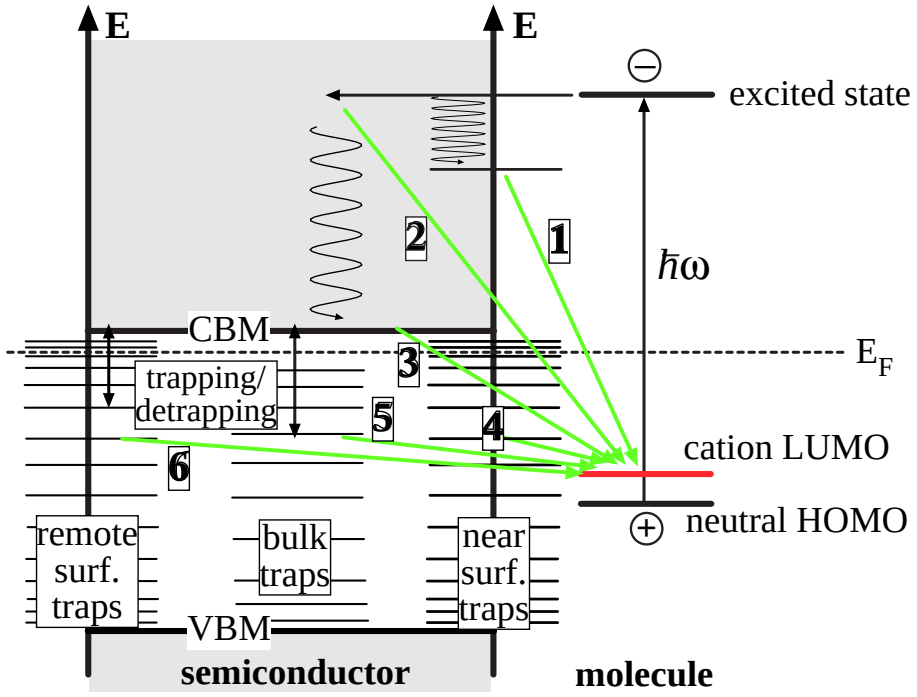

Figure 4.26: Schematic illustration of possible recombination channels after electron injection: from a temporarily occupied surface state (1), from hot injected electrons prior or during the relaxation process (2), from a relaxed or temporarily detrapped electron at the CBM (3), or from near traps (4), bulk traps (5), or remote traps (6).

revealed that the Fermi level is close to the CBM during the measurement (section 3.4.2). It has been discussed that this is not the dark equilibrium level but rather a quasi-equilibrium level due to the filling of the trap states between the true Fermi level and the CBM. The filling of the trap states provides the photovoltage in a working DSSC [149, 6, 151]. As the irradiation during the pump-probe measurement exceeds that of the solar spectrum by a few hundred, it is plausible that the trap states are filled close to the CBM during the pump-probe experiment.

J. Nelson *et al.* [232, 233] and A. Barzykin and M. Tachiya [234] developed random-flight models, which are based on the assumption that electrons undergo fast detrapping in the semiconductor. While being the conduction band, the electrons are delocalized and may be localized again (after a "random flight") in another trap state or recombine with the cation. This mechanism is included in channel (3) in Fig. 4.26. These models qualitatively reproduce experimental results by Durrant and co-workers [228], who observed a dependence of the kinetics on the light intensity. However, Hagfeldt and co-workers observed an independence of the recombination kinetics from the pump intensity for a very similar system [20]. The random-flight models are also inconsistent with recent THz-spectroscopy measurements [230]. According to unpublished data of R. Eichberger, C. Zimmermann and F. Willig, the

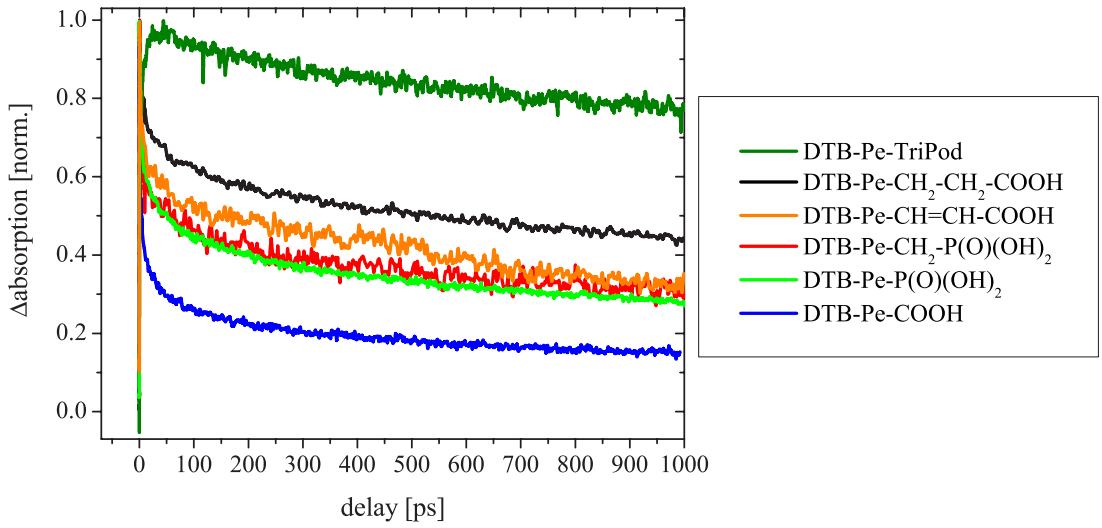

Figure 4.27: Recombination kinetics for all investigated perylene dyes in UHV. The graph shows the transient absorption at 570 nm.

recombination kinetics of DTB-Pe-CH_2-P(O)$(OH)_2$ shows only a very weak temperature dependence. This contradicts a detrapping mechanism as well, as this process would be thermally activated.

If the cation does not recombine with a detrapped electron, the final recombination path is nuclear tunneling from a localized state. Assuming a uniform distribution of the trap states, the difference between the reactant states ranges from next-neighbor up to the diameter of the colloids (if inter-colloid tunneling is neglected). The distribution in the distances is illustrated as channels (4)-(6). Such a tunneling mechanism has been proposed as the origin of "impurity conductivity" of semiconductors in the 1950's (see Ref. [235] and references therein). The weak temperature-dependence of tunneling processes is in qualitative agreement with the mentioned experimental results of R. Eichberger *et al.*

An important property for any recombination channel is the energetic position of the acceptor state. The LUMOs of perylene are about 1 eV (β) and 1.5 eV (α) above the neutral HOMO, and thus about 1 eV and 0.5 eV below the CBM. Assuming that the quasi-Fermi level shifts under illumination by 800 meV (typical open-circuit voltage of the DSSC), already the intrinsic occupation of the semiconductor is above the β-LUMO. Therefore, the cation may also be reduced by so-called alien recombination, i.e. by an electron, which has not been injected before. The UPS spectra of Fig. 3.12 show in fact a small signal throughout the whole band gap, which is in agreement with Ref. [175], indicating occupied trap states up to the Fermi level.

Fig. 4.27 shows the decay of the cation absorption within the first nanosecond for all investigated perylene dyes. Obviously, the trends observed for the early re-

combination persist. Interestingly, also on this long time scale DTB-Pe-CH=CH-COOH shows similar kinetics as DTB-Pe-CH_2-CH_2-COOH, which is indicated already within the first 500 fs.
Both perylene-phosphonic acids show very similar recombination kinetics in Fig. 4.27. However, it should be noted that different samples of the same dye-TiO_2 system show a larger spread in the recombination kinetics compared to the electron injection. The decay curves have been fitted with multi-exponential functions. In the case of DTB-Pe-tripod, the signal can be fitted with two exponentials resulting in time constants of 170 ps (10%) and 6.8 ns (90%). The fit of the fastest decay curve (DTB-Pe-COOH) requires at least three time constants, which reach from sub-picossecond to nanoseconds (700 fs (37%), 25 ps (33%), 1.6 ns (30%)). It should be mentioned that this multi-exponential fits are not based on any physical model. Also the differences in the decay curves between the various dyes do not give any evidence on the recombination channel. However, the dependence shown in Fig. 4.27 clearly states that the electronic interactions relevant for the back ET have to be considered in the recombination models.

4.4.2 Reproducibility of the measurements - Diffusion of sodium from the glass substrate

In the previous sections, the dependence of the electron injection kinetics on the interfacial electronic coupling has been discussed in terms of the molecular properties. The electronic structure of the semiconductor has been assumed as a "black box", i.e. as a constant for all different perylene dyes. However, the microscopic properties of nano-structured solids, in particular metal oxides, is known to be sensitive on many parameters of the preparation procedure [135, 133, 236]. Therefore, the unambiguous assignment of features of the pump-probe signals to differences of the molecular properties requires multiple measurements of the same system. In the coarse of this thesis, around 200 samples have been prepared, from which more than 100 were investigated with pump-probe spectroscopy. In the previous sections, for each dye-anatase system only a single time trace was presented. However, each system was investigated for several independent samples. The given uncertainties in the time constants were estimated from the spread obtained from the repeated measurements.

In view of the correlation between coupling and injection time, it is not astonishing that changes in the colloid preparation result in different kinetics. However, it has been observed that also the choice of the glass substrate effects the coupling of the adsorbate to the surface.

As example, Fig. 4.28 shows the rise of the cation absorption of DTB-Pe-CH_2-CH_2-

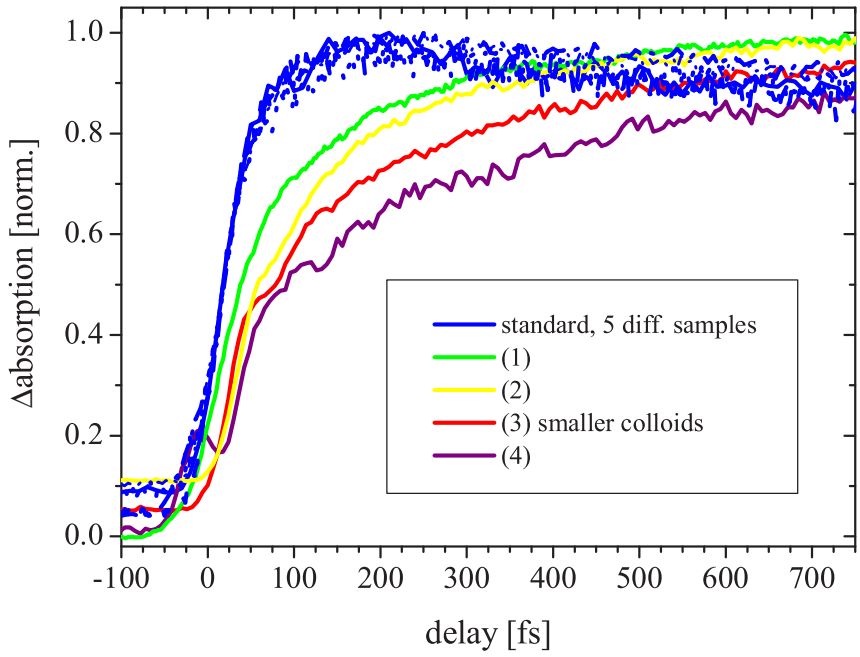

Figure 4.28: Transient cation absorption at 570 nm of DTB-Pe-CH_2-CH_2-COOH for different anatase samples. The electron injection kinetics shows a strong dependence on the preparation procedure and on the choice of the glass substrate. The pump-probe signals given as blue lines correspond to five different samples with AF45 and D263 glass substrates. The substrates of the other samples are: 500 nm SnO_2:F on 1 mm float glass (1-3), microscope objective glass (4). The colloid preparation of sample (3) was modified, resulting in smaller colloids.

COOH on different anatase samples. The signals of five different samples on either 40 and 70 μm D263 glass or 50 μm AF45 glass (see section 3.2.2.3) are given as blue lines. These five samples originate from three different colloid preparations following the same procedure. The spread in the injection time constants of these samples is less than 15%. The situation is significantly different for the samples (1)-(4). A conducting substrate (Nippon Sheet Glass, 500 nm SnO_2:F on 1 mm soda-lime glass) has been used for the samples (1)-(3), whereas a 1 mm microscope slide (Electroverre SA, Switzerland) was used for sample (4). Additionally, the colloid preparation of sample (3) followed a different recipe (lower temperature during the autoclaving process), resulting in smaller colloids according to TEM images. This influence of the glass substrate can be observed for any of the perylene chromophores (besides DTB-Pe-tripod, for which this effect has not been studied).

The absorption spectrum of the adsorbed dyes is affected by the choice of the glass substrate as well. Fig. 4.29 shows the net dye absorption of DTB-Pe-COOH ad-

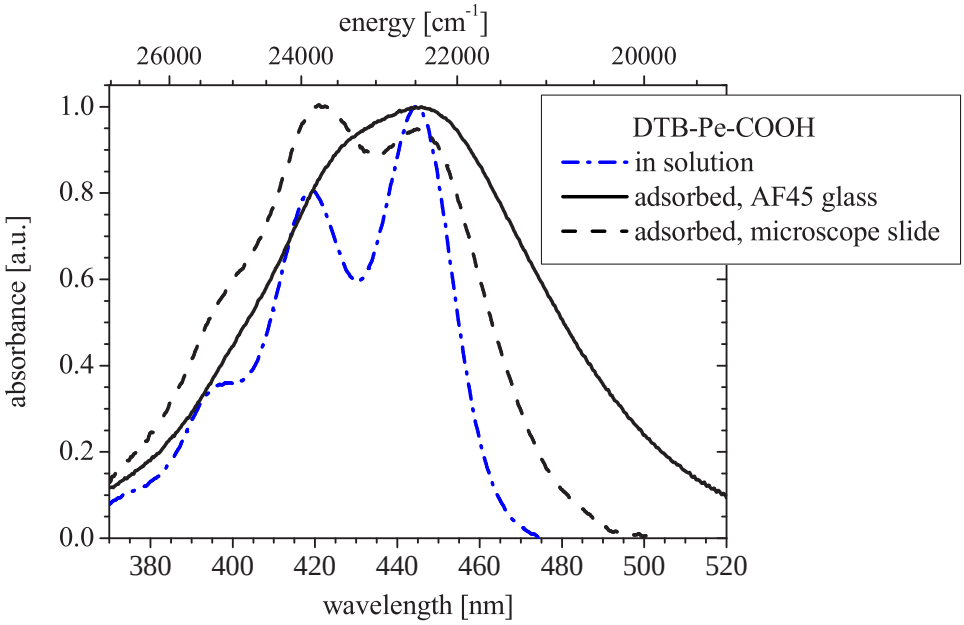

Figure 4.29: Absorption spectrum of DTB-Pe-COOH adsorbed on anatase films prepared on different glass substrates.

sorbed on anatase films prepared on 50 μm AF45 glass (black solid line) and on a 1 mm microscope slide (black dashed line). For comparison, the absorption of the free dye in 1:1 toluene:methanol is given as blue dash-dotted line. Obviously, the electronic coupling of the adsorbate is significantly different.

The significant differences in the electron injection times as well as the absorption spectra can be ascribed to a different dye-surface bonding due to the presence of alkali atoms, mainly sodium, at the surface. The porous films are prepared by a temperature treatment (450 °C, 1 hour) of a Carbowax-colloid mixture, which has been deposited on a glass substrate (section 3.2.2.1). Alkali atoms are known to have a high mobility and to diffuse from the substrate into deposited layers. This effect is known from the preparation of Cu(In,Ga)Se_2 solar cells [237]. Within this technology, the diffusion from Na into the chalcopyrite semiconductor is of essential importance for the growth of the films as well as the electronic properties of the semiconductor.

The migration of sodium from the substrate into a deposited film will certainly depend on the sodium content, but also in addition on the mobility within a particular glass type. The content of sodium oxide (Na_2O) in the microscope slides is 14.3% (information from Electroverre SA, Switzerland), in comparison to 6.4% for D263 and <0.2% for AF45. In the case of the SnO_2:F/soda-lime substrate, the sodium oxide content of soda-lime glass is in the range of 12 to 18%. As can be seen from Fig. 4.28, usage of the microscope slide reduces the injection time more compared

to the conducting glass substrate. The conducting SnO_2:F layer probably acts as a partial diffusion barrier resulting in a lower sodium concentration in the anatase film.

The assignment of the origin of the effects to the presence of sodium is confirmed by two measurements:

- Two pieces of conducting glass have been tempered at 450 °C for 1 hour on a microscope slide. The conducting SnO_2:F layer of one of the samples faced the microscope slide, the other one was reversed. Subsequent XPS measurements of both pieces show a significantly enhanced Na 1s peak on the surface facing the microscope slide.

- Sodium oxide was added to the Carbowax-colloid mixture prior to the burning of the film on AF45 glass. SEM images of the anatase film as wells as TEM images of single colloids do not show any difference to the standard samples for Na_2O concentrations of 0.1% and 0.3%. However, the electron injection kinetics as well as the absorption spectrum of DTB-Pe-COOH adsorbed on this films show the same features as for the films prepared on microscope slides without the addition of sodium oxide.

The differences in the adsorbate-surface binding due to the presence of sodium have not been unambiguously clarified. It is plausible that the carboxylate group interacts with the sodium ion (see Ref. [170] and references therein) rather than titanium surface atoms, resulting in a saline Na^+-Pe-COO^- complex. In this situation, the interaction of the carboxylate group with the surface is reduced. This assumption is in agreement with the calculations of Vittadini *et al.* [166] and the observation that the dyes can be partialy detached from a sensitized film by rinsing it with methanol. The sensitization of the films is realized by immersion of the films in a dye-toluene solution, i.e. by preparation in a nonpolar solvent. The sensitization process does not show a dependence on the presence of sodium in the film. However, rinsing of the sensitized films with a polar solvent dissolves the Na^+-Pe-COO^- complex, contrary to Na-free sensitized films. The anatase films prepared with the addition of Na_2O decolor completely in methanol.

This observed dissociation is relevant for the DSSC. One of the origins of degradation of DSSC is the dissolution of the dye molecules [238]. Ru-complexes have poor photostability as free dyes in solution due to the reactivity of the excited triplet state. Therefore, a reduction of the sodium content in the porous anatase films might enhance the strength of the adsorbate-surface binding and improve the long-term stability of the DSSC.

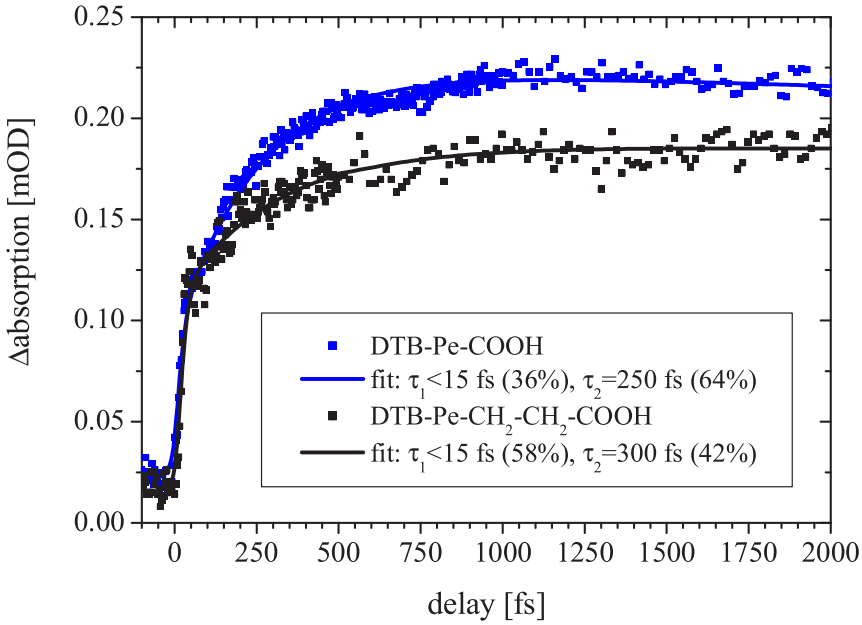

Figure 4.30: The kinetics of electron injection from DTB-Pe-COOH and DTB-Pe-CH_2-CH_2-COOH into nano-structure ZnO probed by transient cation absorption at 570 nm. Both signals show a bi-exponential rise with one very fast time constant (see inset).

4.4.3 Electron injection into ZnO

Although ZnO has a very similar band gap and similar band edge positions with respect to vacuum compared to TiO_2 [6, 239], DSSC based on this metal oxide show only a poor performance [16, 20]. Lian and co-workers [16], Hagfeldt and co-workers [20] and Furube and co-workers [240] investigated the injection and recombination kinetics of adsorbed Ru-complexes on ZnO. Lian *et al.* reported a significant slower injection into ZnO compared to TiO_2 and explained this observation in terms of a lower DOS in the ZnO conduction band.
To verify this argument, the electron injection of DTB-Pe-COOH and DTB-Pe-CH_2-CH_2-COOH into ZnO has been investigated. The synthesis of the ZnO colloids followed the procedure described in Ref. [241]. Nano-structured films have been prepared analogous to the anatase films by use of carbowax and a subsequent temperature treatment.

The kinetics of the electron injection from DTB-Pe-COOH and DTB-Pe-CH_2-CH_2-COOH are shown in Fig. 4.30. Both transient cation signals show a bi-exponential rise. Interestingly, both dyes partially inject with one ultrafast time constant. The FWHM of the CC was 38 fs in this experiment, which was not sufficient to resolve

the initial rise. According to the data fitting with the rate equation model, the upper limit can be estimated to be 15 fs for both chromophores. Also the difference in the second time constant of both pump-probe signals is remarkably small. This injection kinetics significantly differ from electron injection into TiO_2, however not in the same manner as reported by Lian *et al.* [16]. The ultrafast component of the injection kinetics rules out a significantly lower density of acceptor states compared to TiO_2.
Furube and co-workers observed a multi-exponential electron injection as well, with a fast component below 100 fs and several slower components of up to 1 ns [240]. These observations has been interpreted in terms of stepwise electron injection, first into a surface state (<100 fs), which decays slowly into bulk states.

The chemical stability of ZnO is know to be poorer compared to TiO_2. For instance ZnO nano-particles are dissolved by acetic acid [242]. Hagfeldt and co-workers observed a correlation between the performance of the sample as photovoltaic device and the injection kinetics [20]. Efficient solar cells showed fast injection (<300 fs).

The combination of these different observations suggest that the sensitizers, which all exhibit carboxylic groups as anchors, partially dissolve the nano-structured ZnO and form salt complexes. Under UHV conditions, very loosely bound complexes desorbe and leave the system. In solution, however, the complexes stay in the pores of the porous film.

In conclusion, the ET kinetics shown in Fig. 4.30 reveal that electron injection into ZnO can occur on the same time scale compared to TiO_2. However, due to the surface chemistry of ZnO, the system appears to be less defined.

4.4.4 Solvent effects on the electron transfer

At the end of this thesis, the influence of a solvent environment on the kinetics of interfacial ET is briefly considered. This topic is an interesting aspect of heterogeneous ET, as in any technological relevant system a solid state environment will be present. However, from the scientific point of view, the elaboration of the solvent effects requires the understanding of the system under UHV conditions. Therefore, this thesis provides the basis for the investigation of solvent effects: first, with respect to the achieved understanding of the ET process in UHV, and secondly by the development of the UHV-gas-liquid chamber, which allows the introduction of a solvent at a high purity grade. The remaining of this section gives a survey of the possible types of solvent effects and presents some exemplary measurements.

Hitherto, theoretical calculations of through-bond electronic interaction [43, 44, 46, 218, 45, 47, 48, 49, 50, 51, 52, 31] have been compared only to measurements that

were carried out in a solvent environment and with molecular donor-acceptor pairs. Electronically saturated molecular bridge groups usually have no unoccupied electronic states below the vacuum levels, i.e. these bridges have negative electron affinity. It is controversially discussed, to which extent the molecular bridge ("through-bridge") or the vacuum levels ("through-space") mediate the electronic interaction in such a situation [63, 43, 44, 46, 56, 45].

Recently, Zimmt, Waldeck and co-workers addressed this question indirectly by studying the ET kinetics in C-shaped donor-bridge-acceptor systems [64, 65]. These molecules show a cleft between donor and acceptor, into which solvent molecules can penetrate. These authors observed an increase of the electronic interaction with increasing electron affinity of the solvent, which indicates a significant through-solvent coupling.
In the case of homogeneous ET, the environment may affect the ET rate (Eq. 1.2) by changes of the strength of the electronic interaction or of the Franck-Condon factors of the reaction. The separation of theses two contributions is difficult and requires further assumptions [64].
Heterogeneous ET lends itself to address this question, as in the "wide band limit" the injection kinetics directly reflect the electronic coupling, and no Franck-Condon factors have to be considered. This holds also for a solvent environment, as long as the donor level is not significantly lowered in energy by the environment. Additionally, the samples can be brought to vacuum for comparison, which is not easily realizable for a donor-bridge-acceptor molecule.

Fig. 4.31 shows the transient cation signal of DTB-Pe-COOH adsorbed on anatase under UHV conditions as well as in n-hexane. These exemplary measurements should be seen as proof of principle of the technique. The measurement under UHV conditions was performed with the cuvette inside the chamber around the sample (see Fig. 2.1). After this measurement, the chamber was filled with Ar and the dried solvent was brought into the cuvette around the sample as described in detail in section 2.1. The left panel shows the kinetics of the electron injection for both environments. The signal taken in n-hexane is shifted in time to compensate the shift in time-zero induced by the solvent.

The electron injection kinetics remain unchanged, as shown in the left panel. This is in agreement with the expectation, as this dye couples strongly and the small distance between adsorbate and surface does no solvent molecule allow to penetrate between adsorbate and surface. However, it should noted that the FWHM of the CC in this measurements was around 45 fs, which does not allow to resolve small changes of a 15 fs-kinetics. Additional, marginal differences in the rise of the signal can arise from changes of the pulse durations due to the solvent. Interestingly, the onset of the recombination shows a significant difference and the recombination in n-

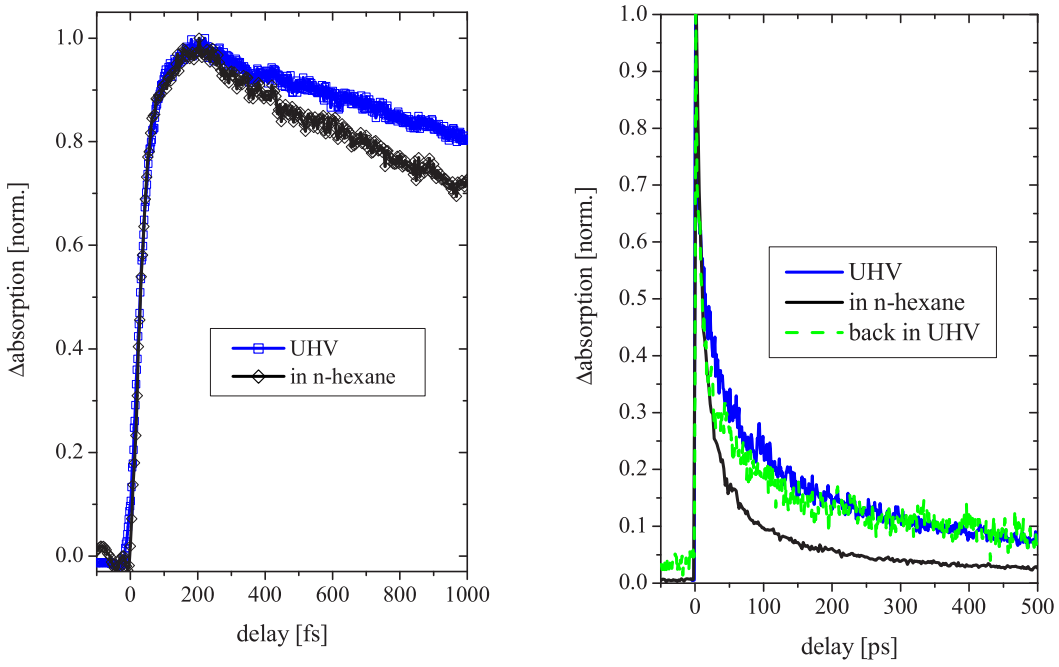

Figure 4.31: Influence of a solvent environment on interfacial ET for DTB-Pe-COOH on anatase. Transient absorption signal at 570 nm of DTB-Pe-COOH on anatase in UHV (blue lines) and in n-hexane (black lines). Left panel: The transient absorption signal of the sample in n-hexane is shifted in time to compensate for the shift in time-zero induced by the solvent and the cuvette. Right panel: The green line in the right panel shows the recombination kinetics 15 h after the samples was brought back to UHV. All curves are normalized.

hexane being faster. This trend continues for the whole decay of the signal, as shown on the right hand side of Fig. 4.31. Bi-exponential fits (with offset) to the signal starting at 1 ps reveal time constants of 15 ps (58%) and 180 ps (37%) for UHV, and 10 ps (73%) and 100 ps (23%) for n-hexane. The green curve shown in the right panel is the recombination of the same sample after bringing the system back to UHV and pumping over night. The sample turns back to its initial condition, which demonstrates that the environment of a sample indeed can be reversibly switched within this chamber.

The full understanding of the solvent effects on interfacial ET requires further measurements with systematically exchanged solvents and dyes. Preliminary results on the DTB-Pe-tripod/anatase system reveal a solvent dependence also of the electron injection kinetics. Thus, future investigations can address the importance of through-bond, through-space and through-solvent contributions to the over-all strength of the electronic coupling.